REPORT DOCUMENTATION PAGE

Form Approved OMB NO. 0704-0188

1. REPORT DATE (DD-MM-YYYY)	2. REPORT TYPE	3. DATES COVERED (From - To)
21-07-2016	Final Report	1-Aug-2012 - 30-Apr-2016

4. TITLE AND SUBTITLE
Final Report: Amphiphilic Block Copolymer Mediated Self-Assembly of Nanocomponents Into Active Metamaterial Structures: Nonlinear Metamaterials

5a. CONTRACT NUMBER
W911NF-12-1-0333

5b. GRANT NUMBER

5c. PROGRAM ELEMENT NUMBER
611102

6. AUTHORS
Philip A. Sullivan, Ph.D.

5d. PROJECT NUMBER

5e. TASK NUMBER

5f. WORK UNIT NUMBER

7. PERFORMING ORGANIZATION NAMES AND ADDRESSES
Montana State University
309 Montana Hall
PO Box 2470
Bozeman, MT 59717 -2470

8. PERFORMING ORGANIZATION REPORT NUMBER

9. SPONSORING/MONITORING AGENCY NAME(S) AND ADDRESS (ES)
U.S. Army Research Office
P.O. Box 12211
Research Triangle Park, NC 27709-2211

10. SPONSOR/MONITOR'S ACRONYM(S)
ARO

11. SPONSOR/MONITOR'S REPORT NUMBER(S)
62059-CH.3

12. DISTRIBUTION AVAILIBILITY STATEMENT
Approved for Public Release; Distribution Unlimited

13. SUPPLEMENTARY NOTES
The views, opinions and/or findings contained in this report are those of the author(s) and should not contrued as an official Department of the Army position, policy or decision, unless so designated by other documentation.

14. ABSTRACT
High-level theoretical analysis tools have been developed and employed in order to better understand the parameter space relevant to the design of hybrid organic/metal-nanoparticle meta-elements and –materials. The first results from this work were published in Applied Physics Letters 103, 031102 (2013). These data have been translated to guide the goals of material synthesis efforts. Materials synthesis to date has consisted of learning to prepare and modify nonlinear dyes, block copolymers, gold nanorods, and functionalized surfaces to yield desired optical/physical properties. Gold nanorods of various length/width aspect ratios (with correspondingly varied

15. SUBJECT TERMS
Nonlinear Metamaterials, NIR absorbers, Nanoengineering, Engineered Optical Properties

16. SECURITY CLASSIFICATION OF:			17. LIMITATION OF ABSTRACT	15. NUMBER OF PAGES	19a. NAME OF RESPONSIBLE PERSON
a. REPORT	b. ABSTRACT	c. THIS PAGE			Philip Sullivan
UU	UU	UU	UU		19b. TELEPHONE NUMBER 406-994-5692

Report Title

Final Report: Amphiphilic Block Copolymer Mediated Self-Assembly of Nanocomponents Into Active Metamaterial Structures: Nonlinear Metamaterials

ABSTRACT

High-level theoretical analysis tools have been developed and employed in order to better understand the parameter space relevant to the design of hybrid organic/metal-nanoparticle meta-elements and –materials. The first results from this work were published in Applied Physics Letters 103, 031102 (2013). These data have been translated to guide the goals of material synthesis efforts. Materials synthesis to date has consisted of learning to prepare and modify nonlinear dyes, block copolymers, gold nanorods, and functionalized surfaces to yield desired optical/physical properties. Gold nanorods of various length/width aspect ratios (with correspondingly varied optical properties) have been successfully functionalized with multi-block copolymers and/or alkane-thiol functionalized ONLOs. The unique linear optical properties of these materials demonstrate potential utility in mitigating long-standing efficiency problems in compact YAG laser designs. A publication detailing these results has been accepted for publication in ACS Applied Materials and Interfaces (Jul. 2016). Vertical nanorod (nanopillar) array samples from the Anatoly Zayats research lab at Kings College, London have also been functionalized with ONLOs and analyzed.(6) Nonlinear effects resulting from these efforts are being evaluated using Sum Frequency Generation (SFG) and Second Harmonic Generation (SHG) in collaboration with Professor Robert Walker's Lab at MSU.

Quite promising results have been realized through direct covalent attachment of alkane-thiol functionalized ONLOs within vertical nanorod arrays. SFG data confirms the existence of large ?(2) without external symmetry breaking (electric field poling). Additionally, when these samples are compared with ONLOs attached to flat gold surfaces, using polarization resolved SFG, quite different nonlinear optical behavior is observed. Specifically, in the case of ONLO interspersed vertical nanorod array samples, orthogonally polarized visible (801 nm) and IR (3250 nm) optical inputs give rise to large SFG signals. In contrast only parallel polarized visible and IR inputs give rise to significant SFG in the case of ONLOs attached to flat (unstructured) gold surfaces. These results are potentially very significant, proving that hybrid nanostructured NLMMs can yield large ?(2) responses and suggesting that appropriately designed NLMMs may be used to introduce non-natural effective ?(2) tensor elements. A publication detailing these results is currently in preparation.(6)

Enter List of papers submitted or published that acknowledge ARO support from the start of the project to the date of this printing. List the papers, including journal references, in the following categories:

(a) Papers published in peer-reviewed journals (N/A for none)

Received	Paper
07/21/2016	2 Ryan E. Latterman, Steven Birrell, Philip A. Sullivan, Robert A. Walker. Improved pulsed laser operation with engineered nanomaterials, ACS Applied Materials and Interfaces, ( ): . doi:
TOTAL:	**1**

Number of Papers published in peer-reviewed journals:

(b) Papers published in non-peer-reviewed journals (N/A for none)

Received Paper

TOTAL:

Number of Papers published in non peer-reviewed journals:

(c) Presentations

Number of Presentations: 0.00

Non Peer-Reviewed Conference Proceeding publications (other than abstracts):

Received Paper

TOTAL:

Number of Non Peer-Reviewed Conference Proceeding publications (other than abstracts):

Peer-Reviewed Conference Proceeding publications (other than abstracts):

Received Paper

TOTAL:

Number of Peer-Reviewed Conference Proceeding publications (other than abstracts):

(d) Manuscripts

Received Paper

TOTAL:

Number of Manuscripts:

Books

Received Book

TOTAL:

Received Book Chapter

TOTAL:

Patents Submitted

Patents Awarded

Awards

Graduate Students

NAME	PERCENT_SUPPORTED	Discipline
Ryan Latterman	1.00	
Ky Michelson	0.50	
FTE Equivalent:	**1.50**	
Total Number:	**2**	

Names of Post Doctorates

NAME	PERCENT_SUPPORTED
FTE Equivalent:	
Total Number:	

Names of Faculty Supported

NAME	PERCENT_SUPPORTED	National Academy Member
Philip A. Sullivan, Ph.D.	0.30	
FTE Equivalent:	**0.30**	
Total Number:	**1**	

Names of Under Graduate students supported

NAME	PERCENT_SUPPORTED
FTE Equivalent:	
Total Number:	

Student Metrics

This section only applies to graduating undergraduates supported by this agreement in this reporting period

The number of undergraduates funded by this agreement who graduated during this period: 3.00

The number of undergraduates funded by this agreement who graduated during this period with a degree in science, mathematics, engineering, or technology fields:..... 3.00

The number of undergraduates funded by your agreement who graduated during this period and will continue to pursue a graduate or Ph.D. degree in science, mathematics, engineering, or technology fields:..... 0.00

Number of graduating undergraduates who achieved a 3.5 GPA to 4.0 (4.0 max scale):..... 3.00

Number of graduating undergraduates funded by a DoD funded Center of Excellence grant for Education, Research and Engineering:..... 0.00

The number of undergraduates funded by your agreement who graduated during this period and intend to work for the Department of Defense 0.00

The number of undergraduates funded by your agreement who graduated during this period and will receive scholarships or fellowships for further studies in science, mathematics, engineering or technology fields:..... 0.00

Names of Personnel receiving masters degrees

NAME
Total Number:

Names of personnel receiving PHDs

NAME
Ryan Latterman
Total Number: 1

Names of other research staff

NAME	PERCENT_SUPPORTED
FTE Equivalent:	
Total Number:	

Sub Contractors (DD882)

Inventions (DD882)

Scientific Progress

Gold nanorods of various length/width aspect ratios (with correspondingly varied optical properties) have been successfully functionalized with multi-block copolymers and/or alkane-thiol functionalized ONLOs. The unique linear optical properties of these materials demonstrate potential utility in mitigating long-standing efficiency problems in compact YAG laser designs. A publication detailing these results has been accepted for publication in ACS Applied Materials and Interfaces (Jul. 2016). Quite promising results have been realized through direct covalent attachment of alkane-thiol functionalized ONLOs within vertical nanorod arrays. SFG data confirms the existence of large ?(2) without external symmetry breaking (electric field poling). Additionally, when these samples are compared with ONLOs attached to flat gold surfaces, using polarization resolved SFG, quite different nonlinear optical behavior is observed. Specifically, in the case of ONLO interspersed vertical nanorod array samples, orthogonally polarized visible (801 nm) and IR (3250 nm) optical inputs give rise to large SFG signals. In contrast only parallel polarized visible and IR inputs give rise to significant SFG in the case of ONLOs attached to flat (unstructured) gold surfaces. These results are potentially very significant, proving that hybrid nanostructured NLMMs can yield large ?(2) responses and suggesting that appropriately designed NLMMs may be used to introduce non-natural effective ?(2) tensor elements. A publication detailing these results is currently in preparation. Further details can be found in the report included in the attachment section.

Technology Transfer

Engineered Gold Nanorods were successfully used to improve the efficiency of compact YAG lasers intended for industrial applications. Please see the "publications" section of this report for more information.

Final Report - Amphiphilic Block CoPolymer Mediated Self-Assembly of Nanocomponents into Active Metamaterial Structures: Nonlinear Metamaterials

Proposal Number: 62059-CH
Agreement Number: W911NF-12-1-0333
Aug. 01, 2013 – Jul. 15, 2016

- **Principle Investigator:** Philip A. Sullivan, *Phone:* 406-994-5692, *Fax:* 406-994-5407,
e-mail: psullivan@chemistry.montana.edu

- **Institution address:** Montana State University
Department of Chemistry and Biochemistry
103 Chemistry and Biochemistry Building, Bozeman, MT 59717-2470

- **Administrative/business contact:** Traci Miyakawa, Senior Fiscal Manager, Montana State University, Office of Sponsored Programs, 309 Montana Hall, Bozeman, MT 59717-2470, *Phone:* 406-994-7696, *Fax:* 406-994-7951, *e-mail:* tracim@montana.edu

- **Duration of effort:** 03/01/2012 – 12/28/2015

Table of contents:

1) Effort Overview

Nonlinear optical metamaterials (NLMMs), are predicted to support novel and anomalous wave-mixing behaviors with promise in optical switching, sensing, and frequency conversion.(1, 2) The current effort aims to prepare and characterize hybrid organic/metal-nanoparticle NLMMs. These metamaterials consist of periodic arrays of anisotropic metallic nanoparticles (nanorods) interspersed with organic nonlinear optical dielectrics (ONLOs). In this research, a number of approaches are being explored in order to: 1) prepare and characterize periodic metal nanorod arrays interspersed with ONLOs; 2) study the interaction of surface plasmon enhanced electric fields with attached ONLOs; 3) prepare new ONLOs designed to spontaneously exhibit enhanced $\chi^{(2)}$ optical nonlinearity. Block-copolymer based organic materials are being explored as a means to simultaneously organize nanoparticle and organic nonlinear optical subunits. Concurrently, vertically oriented nanorod arrays prepared via aluminum film anodization followed by Au electrodeposition, are being studied as an NLMM platform. After preparation of the vertical nanorod arrays, ONLOs are either physically introduced (via electrostatic coating) or covalently bound via gold-thiol reactions.

Theoretical analysis, predicts that hybrid nanostructured NLMMs will yield greatly enhanced effective nonlinear susceptibilities, as well as exquisite control over the directionality of internal local electromagnetic (EM) fields.(3, 4) Such control will allow dramatic differences in the macroscopic (incident) and local (internal) EM fields to be engineered toward manipulation of multiple wave interaction. Such manipulation will enable the combination of enhanced nonlinearity with massive anisotropy, and the introduction of non-natural effective nonlinear tensor elements (see section 2.1).(3) We have recently gathered experimental evidence that appears to confirm a number of these predictions (section 2.2). Designer optical properties, resulting from control over the magnitude and orientation of optical nonlinearities and dispersion characteristics will facilitate, for example, phase matching schemes that could potentially be used to achieve mirrorless optical parametric oscillation/amplification (MOPO/MOPA). MOPA may be used as a route to combat the problematic optical losses (potentially even introducing signal gain) that currently limit the utility of optical metamaterials.(5)

In order to realize the goals stated here, the current research effort must combine the three pillars of an effective rational design process: multi-scale theoretical modeling; material synthesis; and material characterization. To accomplish this, the capabilities of the Sullivan Lab at MSU are being supplemented by collaborative interactions with other world class research groups including: The David R. Smith Lab and the Center for Metamaterials and Integrated Plasmonics (Duke University); The Robert Walker Lab (Montana State University); The Anatoly Zayats Lab and the (EPSRC funded) UK Research Programme on Nanoplasmonics (Kings College, London); The Bruce H. Robinson Lab and the NSF Center on Materials and Devices for Information Technology Research (University of Washington); The David Shelton Lab (University of Nevada Las Vegas).

This document is intended to highlight the progress made over the course of the grant. High-level theoretical analysis tools have been developed and employed in order to better understand the parameter space relevant to the design of hybrid organic/metal-nanoparticle meta-elements and –materials. The first results from this work were

published recently in *Applied Physics Letters* 103, 031102 (2013). These data have been translated to guide the goals of material synthesis efforts. Materials synthesis to date has consisted of learning to prepare and modify nonlinear dyes, block copolymers, gold nanorods, and functionalized surfaces to yield desired optical/physical properties. Gold nanorods of various length/width aspect ratios (with correspondingly varied optical properties) have been successfully functionalized with multi-block copolymers and/or alkane-thiol functionalized ONLOs. The unique linear optical properties of these materials demonstrate potential utility in mitigating long-standing efficiency problems in compact YAG laser designs. A publication detailing these results has been accepted for publication in *ACS Applied Materials and Interfaces* (Jul. 2016). Vertical nanorod (nanopillar) array samples from the Anatoly Zayats research lab at Kings College, London have also been functionalized with ONLOs and analyzed.(6) Nonlinear effects resulting from these efforts are being evaluated using Sum Frequency Generation (SFG) and Second Harmonic Generation (SHG) in collaboration with Professor Robert Walker's Lab at MSU.

Quite promising results have been realized through direct covalent attachment of alkane-thiol functionalized ONLOs within vertical nanorod arrays. SFG data confirms the existence of large $\chi^{(2)}$ without external symmetry breaking (electric field poling). Additionally, when these samples are compared with ONLOs attached to flat gold surfaces, using polarization resolved SFG, quite different nonlinear optical behavior is observed. Specifically, in the case of ONLO interspersed vertical nanorod array samples, orthogonally polarized visible (801 nm) and IR (3250 nm) optical inputs give rise to large SFG signals. In contrast only parallel polarized visible and IR inputs give rise to significant SFG in the case of ONLOs attached to flat (unstructured) gold surfaces. These results are potentially very significant, proving that hybrid nanostructured NLMMs can yield large $\chi^{(2)}$ responses and suggesting that appropriately designed NLMMs may be used to introduce non-natural effective $\chi^{(2)}$ tensor elements. A publication detailing these results is currently in preparation.(6)

Work has also commenced toward the preparation of improved $\chi^{(2)}$ materials for nanocomponent integration (section 2.3 of proposal number 62059-CH). This work seeks to explore the preparation of selected pendant modified ONLO chromophores (PMCs) in order to yield materials with improved (or entirely spontaneous) long-range acentric organization. Such acentric organization will yield improved $\chi^{(2)}$ values that may be directly incorporated into nanostructured hybrid NLMMs. So far, rigid body Monte Carlo computer simulations have been performed to guide PMC structure selection (in collaboration with Professor Bruce H. Robinson at University of Washington). Based on computer simulation results, several new PMC structures have been selected and prepared in our labs at MSU. New chemical methods were developed to enable their preparation. Physical, chemical, and nonlinear optical property analyses are currently underway.

2) Synthesis of Thiol-Functionalized Raft Polymers:

2.1 – Introduction to RAFT: In order to harness the predicted field enhancements (see section 5) of ordered nanorods, methods are needed that allow gold nanorods (GNRs) to self assemble into the optimized structures. It has been shown that ordered liquid

crystalline phases can result from high concentrations of a variety of rod shaped nanoparticles (TiO_2, SnO_2, ZnO, and CdTe) functionalized with diblock copolymers.(7, 8) A polymer shell increases the mobility of highly concentrated nanorod solutions and allows for a size-tunable spacer between the rods. This chapter describes the synthesis of gold reactive polymers with the goals of solubilizing them in organic solutions, introducing Diels-Alder functionality, and increasing their mobility at high concentrations.

Typically, GNRs are synthesized in aqueous solutions and stabilized by charged surfactants. The resulting nanoparticle surface charge restricts the ability to use the particles in organic (non-aqueous) environments like those of most functional devices. Useful methods have been developed to solubilize aqueous solutions of gold nanoparticles in organic solutions by replacing the typical surfactant (CTAB) used to stabilize them with alkanethiols. This functionalization also mitigates the surface charge problems and has been shown to yield nearly zero zeta potentials.(9) Some solubilization methods are more complex than others, but a promising approach uses a relatively simple two-step process.(9) Thiol-terminated polyethylene glycol (PEG-SH) serves as an intermediate stabilization layer that makes the nanoparticles soluble in both water and in organic solvents. The PEG-SH functionalized nanoparticles are then redispersed in a solvent such as tetrahydrofuran and left to react with solutions of thiol-terminated alkanes.

In this report nanorods were solubilized using thiol-functionalized copolymers synthesized by the RAFT (reversible addition-fragmentation chain transfer) technique. Originally developed in 1998 by a team at Australia's federal science agency, CSIRO,(10) the RAFT process has since gained huge popularity for its ability to produce nearly monodisperse multi-block polymers with engineered functionality. In a typical free-radical initiated polymerization, polymer chains are formed very rapidly when monomer concentration is high leading to high molecular weight chains in the early stages of the reaction. New polymer chains are also terminated when a radical from one chain reacts with a radical on another. This kind of uncontrolled polymerization leads to broad molecular weight distribution and very little control towards a target molecular weight. Because RAFT is a living free-radical method, the majority of termination events are eliminated allowing for the control of molecular weight yielding low polydispersity with the added utility of the RAFT agent being the end group of the polymer chains produced.

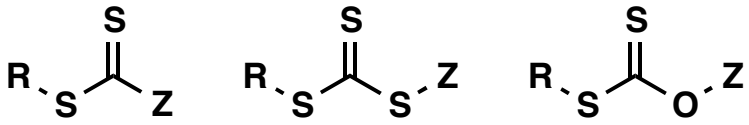

Figure 2.1.1: General structures of common RAFT agents. R is a designed to be both a good leaving group and an efficient free radical reinitiating group. Z should activate the thiocarbonyl towards radical addition.

The RAFT process includes all of the same reagents and conditions used in conventional free-radical polymerization but with the crucial addition of a RAFT chain

transfer agent. The general structure of a RAFT agent is shown in figure 2.1.1 where R is usually an alkyl group that is responsible for reinitiating polymer growth. Z can vary depending on the choice of monomer used in the polymerization and is responsible for activating the double bond in the RAFT agent toward radical addition. Here, the chosen RAFT agent was a trithiocarbonate, a reagent that is especially suitable for acrylate monomers.(11)

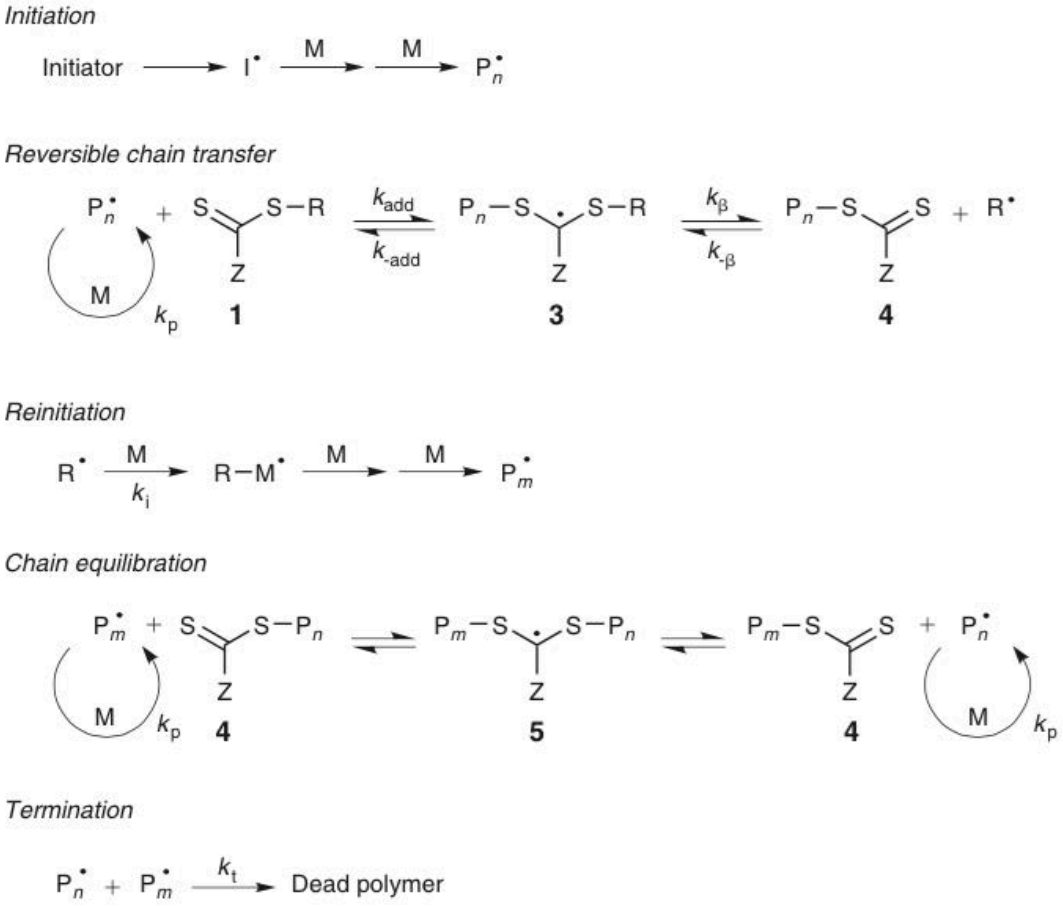

Figure 2.1.2: Generally accepted RAFT mechanism.

All benefits of the RAFT process originate from the addition of a RAFT agent and the unique mechanism resulting from it. Depicted in figure 2.1.2, the mechanism begins with initiation, just as in a typical free-radical polymerization, with a radical produced via an initiator. This radical reacts with a certain amount of monomer to produce an oligomeric radical, $P_n^{\bullet}$. Because the RAFT agents are designed to be reactive, most or nearly all of the added RAFT agent (1) reacts reversibly with the oligomeric radicals, $P_n^{\bullet}$, to form the intermediate radical (3) that can undergo fragmentation to produce a dormant polymer chain (4) along with another radical, $R^{\bullet}$. At this point, reinitiation occurs, and additional monomer reacts with the new radical, $R^{\bullet}$. Polymer chains can thereby grow larger as more monomer is added, but crucially, these new chains react with the RAFT

agent-capped dormant chains (4) in the step labeled "chain equilibrium". Because the radical is effectively sequestered in this equilibrium reaction, termination events are limited, all polymer chains theoretically have the same probability of reacting with a radical, and all of the unique aspects of the RAFT process (low polydispersity, control over molecular weight, RAFT end groups on polymer chains) are observed.

In summary, the RAFT polymerization technique was chosen for this work because of the flexibility it offers with respect to monomer choice, and critically, RAFT allows for facile assembly of block copolymers. RAFT offers the ability to produce polymeric materials with gold-reactive and Diels-Alder reactivity at multiple blocks. Additionally, the RAFT process produces polymers with polydispersities lower than 1.2. In relation to the metamaterial structure proposed (section 5), such capabilities allow for consistent and tunable gap lengths(12) between functionalized gold nanorods while introducing attachment points for nonlinear optical dyes.

2.2 – Synthesis of Thiol-Functionalized PMMA: Figure 2.2.1 shows the first example of a gold-reactive block copolymer synthesized in this work and a depiction of GNRs functionalized with such thiol copolymers. First, methyl methacrylate was polymerized using azobisisobutyronitrile (AIBN) as the radical initiator and 2-cyano-2-propyl dodecyl trithiocarbonate as the RAFT agent. As noted previously, the type of RAFT agent used should be one that is compatible with a desired class of monomer. There are many RAFT agents that work well with acrylic monomers available from commercial sources. One that was adaptable to a variety of different monomer classes was chosen here. This first block of PMMA was not used as a functional center but rather as solubilizing block that

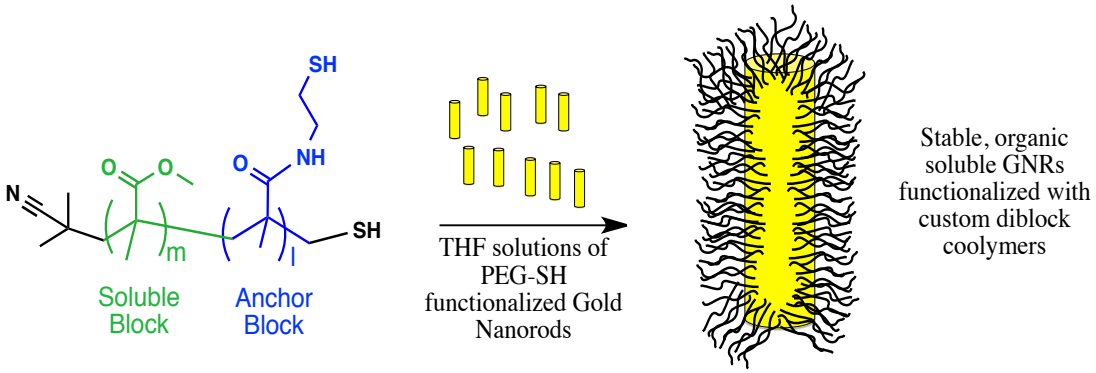

Figure 2.2.1: Summary of GNR functionalization process. GNRs coated in mPEG-SH react with thiol-containing polymer to produce stable organic solutions of GNRs.

contributes to high solubility in organic solvents. The first block is also referred to as the macroinitiator. It contains the RAFT agent at the end of the chain and acts as the initiation site for additional polymerization with another monomer of choice, when initiated using the same radical source (AIBN).

To form the second, reactive block of the diblock copolymer, Pentafluorophenyl methacrylate was next polymerized with this PMMA macroinitator. Pentafluorophenyl methacrylate (PPFMA) was chosen because of its stability during polymerization and the convenient post-functionalization it provides via simple nucleophilic substitution.(7)

After isolating the PMMA-co-PPFMA diblock, treatment with cysteamine produced the gold-reactive diblock copolymer, depicted in figure 2.2.1 as the final product of the synthesis. This simple diblock copolymer was the first material used to functionalize GNRs and solubilize them in organic solvents.

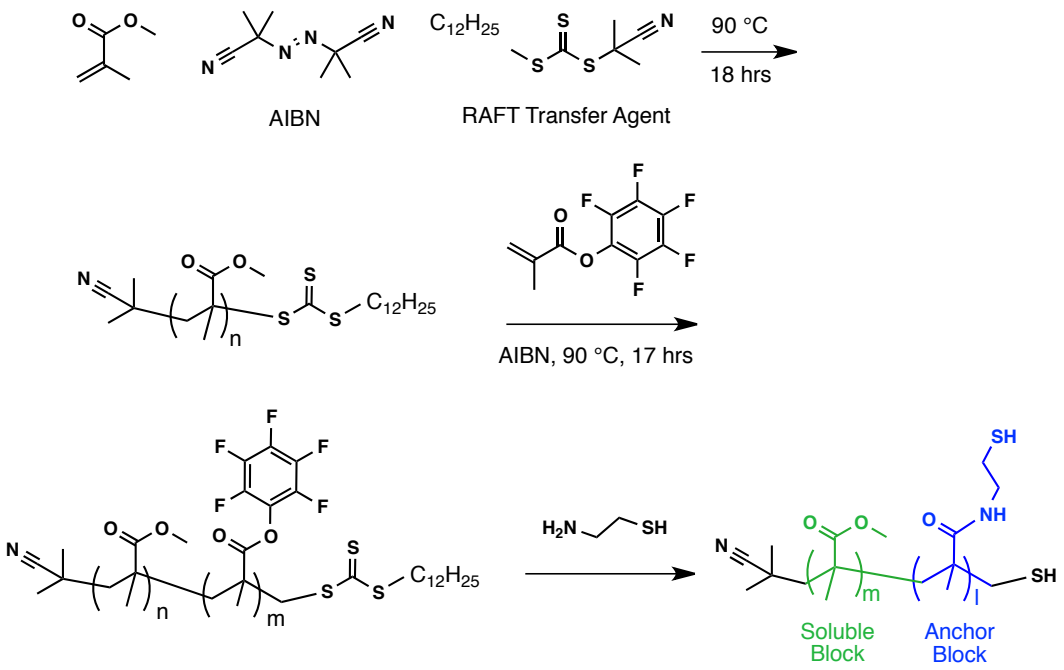

Figure 2.2.1: Synthesis of thiol-containing diblock copolymer.

2.3 – Synthesis of Furan and Anthracene Polymer Derivatives – Scaffolds for Introduction of Nonlinear Organic Dyes: After the synthesis of the basic PMMA/Cysteamine diblock, efforts were focused towards the synthesis of polymers bearing Diels-Alder functionality. The Diels-Alder reaction represents a non-Huisgen "click" reaction that facilitates attachment of a desired compound to a polymer backbone, post-polymerization under mild chemical conditions.(13) In this same manner, it was envisioned that maleimide-functionalized chromophores could be located within the block copolymer "shell" surrounding polymer functionalized GNRs attached for solubilizing the GNRs in organic media. The strategy depicted here was designed so that furan or anthracene bearing monomers would effectively introduce dienes in the block copolymer while maleimide functionality would be introduced as the complementary dieonophile on the desired nonlinear organic chromophores. Figure 2.3.1 depicts an idealized hybrid "meta-atom" composed of dye, gold nanorod and polymer using a furan-containing Diels-Alder polymer. Reaction between furan and maleimide functionality provides a reversible Diels-Alder adduct while the same reaction with anthracene provides an irreversible polymer-dye adduct. Both furan and anthracene polymers were derived from methacrylate monomers and have literature precedence for successful polymerization. We again used acrylic monomers because they are well suited for the chosen RAFT agent.

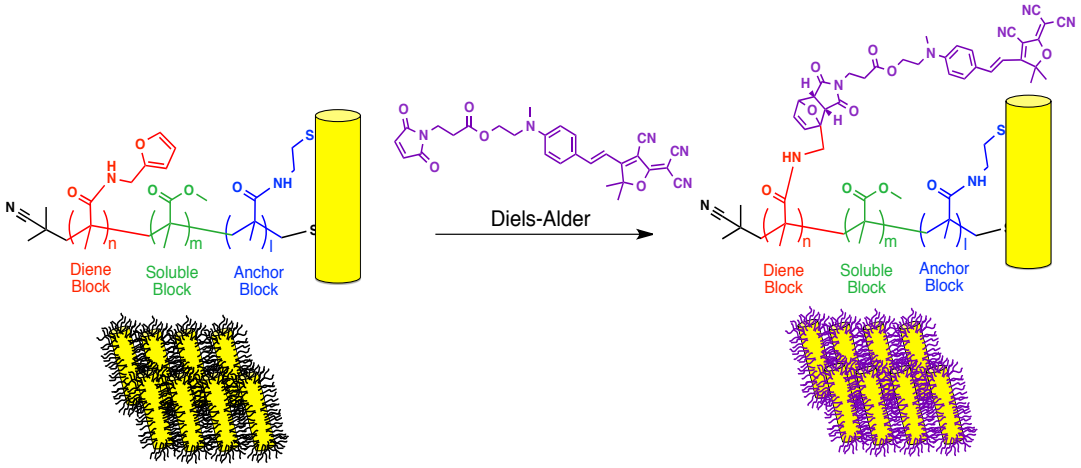

Figure 2.3.1: Ideal GNR-dye hybrid after Diels-Alder reaction between functionalized GNR and nonlinear organic dye.

The first candidate for furan functionality was produced from furfuryl methacrylamide. This monomer was synthesized from furfuryl amine and methacryloyl chloride. Methyl methacrylate and furfuryl methacrylamide were then polymerized together at a specified molar ratio using the typical

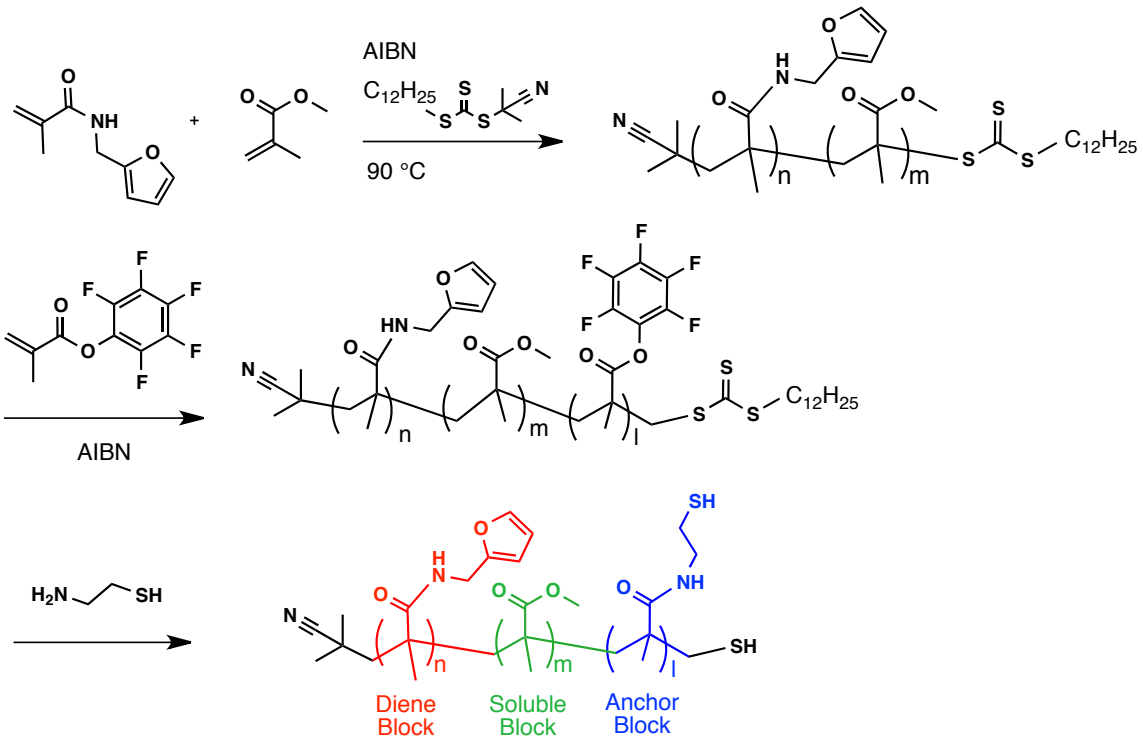

Figure 2.3.2: Synthesis of methacrylamide version of gold-reactive polymer that also contains Diels-Alder functionality.

RAFT protocol to form a random copolymer (RL64, 65). With Diels-Alder reactivity introduced, pentafluorophenyl methacrylate was polymerized with RL64 (RL101) followed by replacement of the pentafluorophenyl group with cysteamine (RL105) to produce a gold-reactive, furan-containing polymer, shown in figure 2.3.2. Eventually, furfuryl methacrylamide was replaced by furfuryl methacrylate because of commercial availability and low cost. Furfuryl methacrylamide was similarly polymerized together with methyl methacrylate but at a specified molar ratio of sixty percent furfuryl

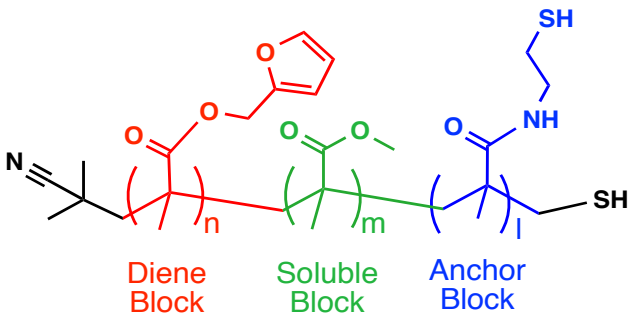

Figure 2.3.3: Revised version of gold-reactive, furan-containing polymer using furfuryl methacrylate rather than furfuryl methacrylamide.

methacrylate to 40 percent methyl methacrylate (RL111, 121). ^{1}H NMR indicated the molar ratio to be very close to what was predicted with 38 percent of the polymer consisting of methyl methacrylate. The copolymer of PMMA and poly(furfuryl methacrylate) was then polymerized with pentafluorophenyl methacrylate and treated with cysteamine to produce the gold-reactive furfuryl methacrylate polymer derivative depicted in figure 2.3.3 (RL117, RL118).

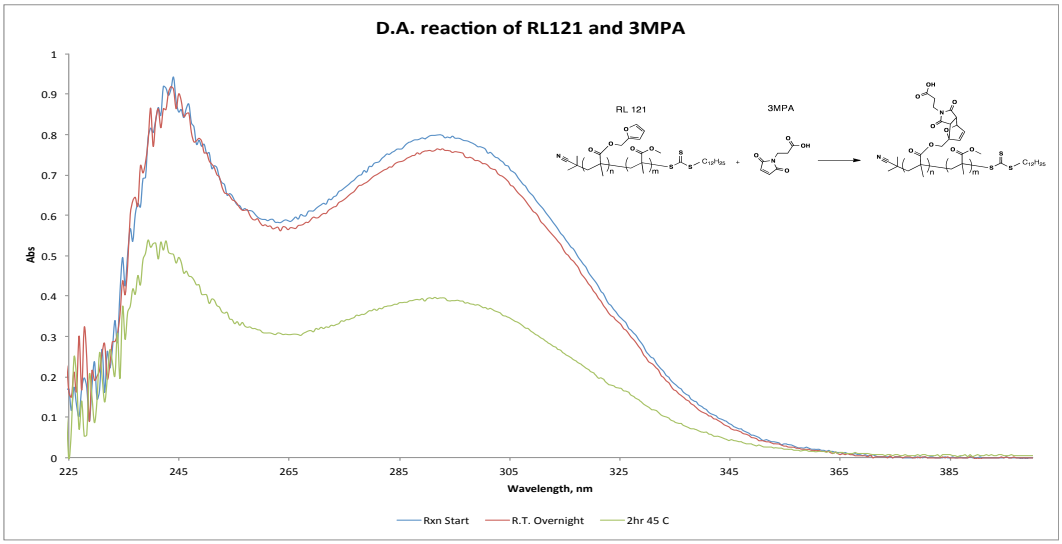

Figure 2.3.4: Diels-Alder reaction between furan-containing RL121 and 3MPA. As the Diels-Alder reaction proceeds, the distinct absorption peak of RL 121 at 290 nm decreases dramatically.

In order to investigate the feasibility of Diels-Alder reactivity, one equivalent (relative to furan monomer) of RL121 was left to react at room temperature overnight with two equivalents of 3-(maleimido)propionic acid (3MPA). 3MPA was used in place of a full dye in order to simplify the absorption spectrum and quickly test the Diels-Alder capabilities of a furan- containing polymer. The furan group on RL121 has a distinct absorption near 290 nm due to its aromatic structure. As a Diels-Alder reaction proceeds, the absorption at 290 nm of the furan group decreases as the conjugation is broken during the formation of a Diels-Alder adduct. Very little absorption change was observed after reacting overnight at room temperature. However, after heating the same reaction mixture for two hours at 45 °C, a large decrease in absorbance was observed, as shown in figure 2.3.4, indicating successful Diels-Alder adduct formation. Thermogravimetric analysis (TGA) was used in further studies to investigate the Diels-Alder reaction between 3MPA and PMMA-co-PFMA

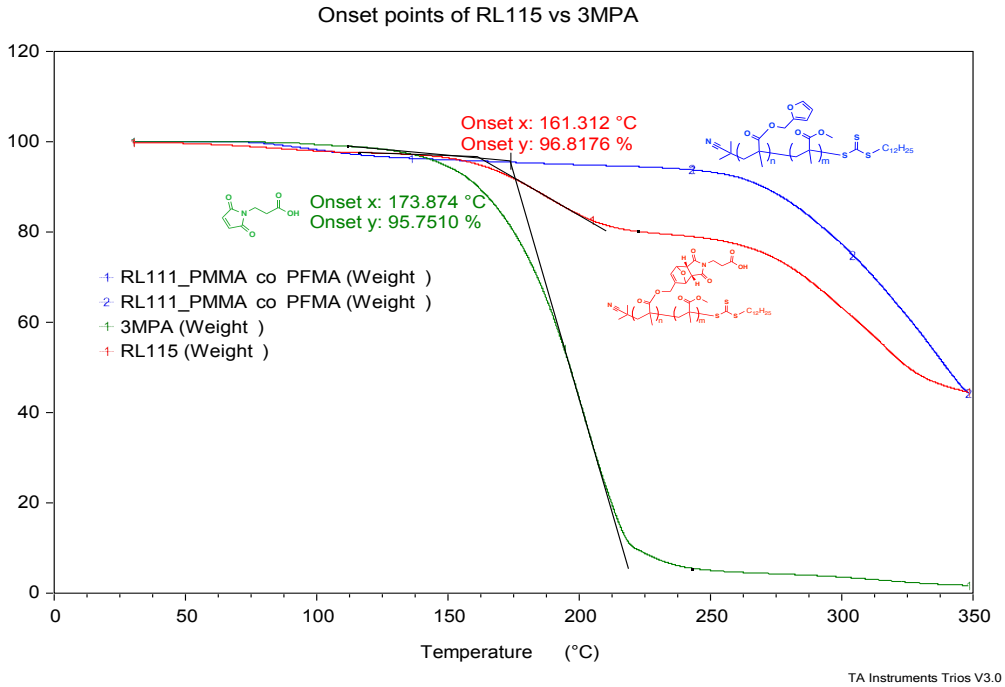

Figure 2.3.5: TGA of Diels-Alder adduct RL115. Pure 3MPA has a distinct decomposition temperature near 170 °C while pure PMMA-co-PFMA shows 275 °C. The Diels-Alder adduct of 3MPA and PMMA-co-PFMA shows loss of mass at 160 °C and 275 °C indicating the loss of 3MPA in a retro Diels-Alder reaction.

polymer. TGA allows for the precise measurement of mass loss as a compound is heated at a specified rate and is often used to study the thermal stability of polymers. The adduct of 3MPA and PMMA-co-PFMA (RL115) was analyzed by TGA and compared to the results of pure 3MPA and PMMA-co-PFMA. Figure 3.9 shows the mass percent vs.

temperature of these three compounds. Pure 3MPA has a fairly sharp onset of mass loss near 170 °C. The Diels-Alder adduct shows a similar but broader onset point. This result may indicate that the 3MPA is being detached from the polymer via a retro-Diels Alder reaction.(14) The adduct also shows mass loss similar to that of pure PMMA-co-PFMA. These results further support the hypothesis that a Diels-Alder reaction between a maleimide-containing dye and a furan-containing polymer should be successful.

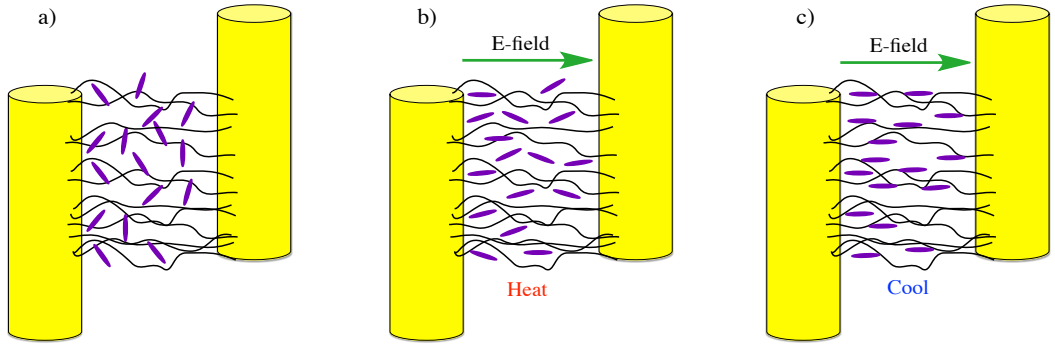

Figure 2.3.6: An idealized depiction of poling of a GNR-polymer-dye hybrid. After functionalizing gold GNRs with polymer and dye, an electric poling field can be used to orient the dyes accentrically in order to produce a non-linear active material. Furthermore, using a reversible Diels Alder adduct may increase chromophore mobility during the heating step.

The furan monomer was chosen because of its ease of synthesis and the fact that a reversible Diels-Alder reaction maybe be beneficial during the poling process (figure 2.3.6), as the GNR-polymer-dye hybrid is heated to the polymer glass transition temperature, the nonlinear dyes should become mobile, due to retro-Diels Alder, and able to reorient parallel to the DC poling field axis creating an acentric (nonlinear optically active) material. As the temperature is decreased, the dyes may covalently re-Diels Alder and re-attach onto the polymers, "locking" acentric order in place. Diels-Alder reversibility may also be eliminated, in case it becomes difficult to control, using i.e. more reactive 9-anthrylmethyl methacrylate instead of the furfuryl version.

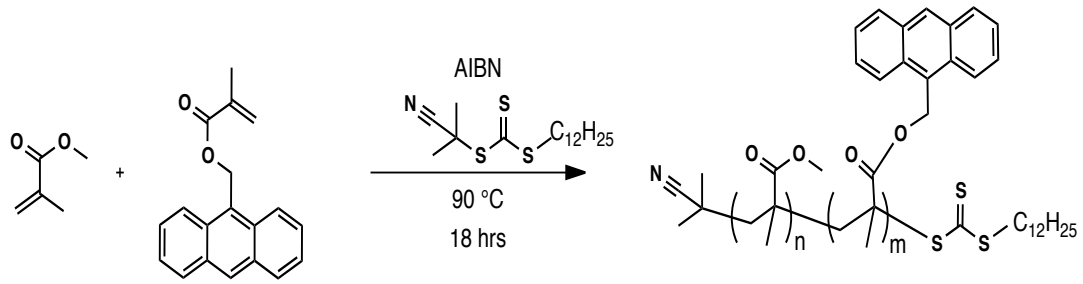

Figure 2.3.7: RAFT Co-polymerization of methyl methacrylate and 9-Anthracenylmethyl methacrylate.

To prepare an anthracene functionalized block copolymer, 9-Anthracene methanol was reacted with methacryloyl chloride to produce 9-Anthracenylmethyl methacrylate (RL 88). In the typical fashion, RL88 was polymerized, in the presence of a RAFT agent, with methyl

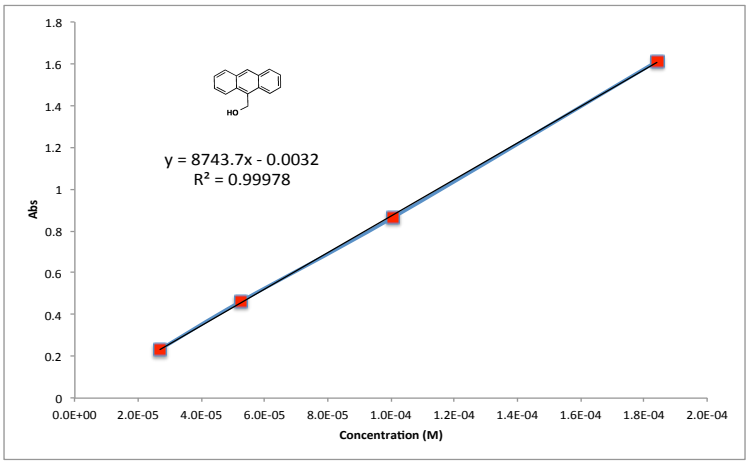

Figure 2.3.8: Calibration curve using 9-Anthracene methanol. Absorption was monitored at 367 nm.

methacrylate to produce a random copolymer block of poly(methyl methacrylate) and poly(9-Anthracenylmethyl methacrylate) (PAnMMA) **(RL89)**. The synthesis scheme is given in figure 2.3.7. In order to calculate actual percentages of anthracene incorporated into the polymer, a UV-Vis absorption calibration curve for the anthracene group was made using solutions of 9-Anthracene methanol as seen in figure 2.3.8. Using this curve, it was determined that RL89 consisted of 11% 9-Anthracenylmethyl methacrylate by mole percent.

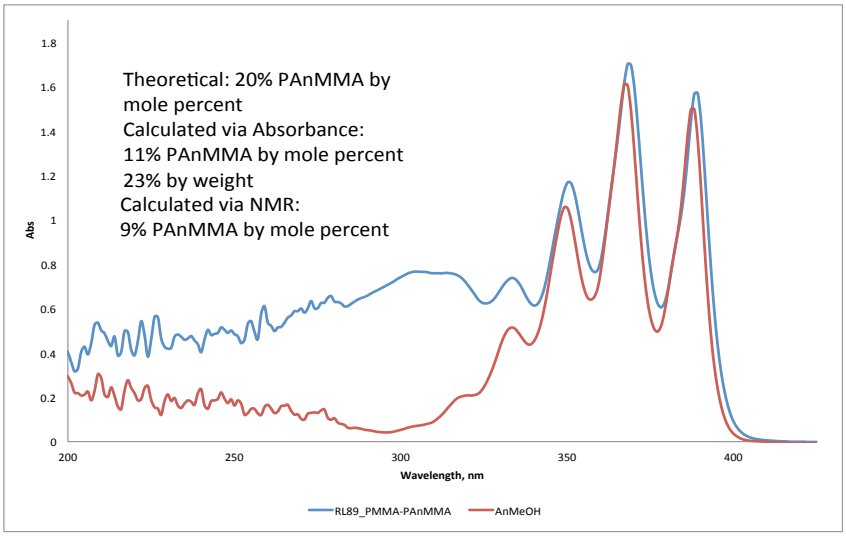

Figure 2.3.9: Absorption spectra of PMMA-co-PAnMMA compared to that of 9-Anthracene methanol.

Similarly, using NMR, it was calculated to be 9% 9-Anthracenylmethyl methacrylate. Figure 2.3.9 summarizes these data and shows the absorption spectra of RL89 polymer compared to 9-Anthracene methanol in tetrahydrofuran.

Similar to the furan derivative, the Diels-Alder reaction between an anthracene group and a maleimide group can be monitored using UV/visible absorption. A slight molar excess of 3MPA was dissolved in dioxane with RL89 and left to react for two hours at 90 °C. Figure 3.14 displays the distinctive absorption profile of the anthracene functional group decreasing as the reaction progresses. These results indicate that an organic dye functionalized with a maleimide group should be a promising candidate for a

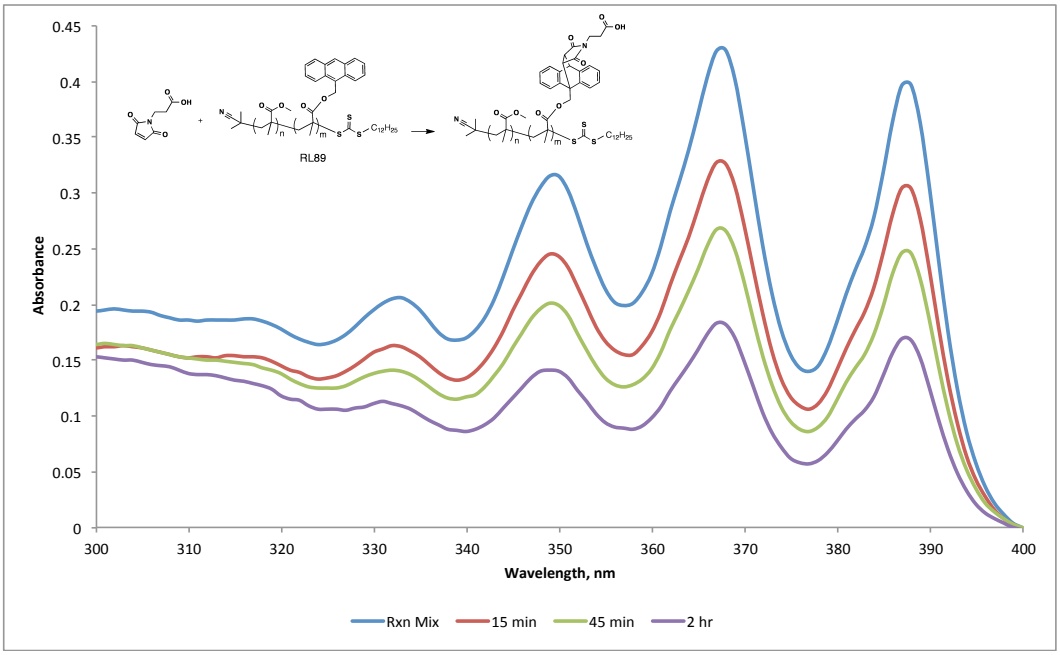

Figure 2.3.10: Diels-Alder reaction of 3MPA with copolymer of poly(methyl methacrylate) and poly(9-Anthracenylmethyl methacrylate). After reacting for 2 hours at 90 °C, a significant loss of anthracene absorption is observed.

Diels-Alder reaction with PAnMMA. Ideally, both the furan and anthracene polymer derivatives will be attached to gold nanorods and then allowed to react with maleimide-containing nonlinear dyes to form the desired hybrid meta-atom.

3) Preparation and Functionalization of Gold Nanorods:

3.1- Gold Nanorod Introduction: Gold nanorods (GNRs) offer a versatile route to the fabrication of tunable metamaterial structures. As discussed in section 5, modeling

results predict large field enhancements between ordered arrays of metallic (silver or gold) nanorods. GNRs were chosen for this application because of their relative ease of synthesis and tunable optical properties. Before the year 2001, GNRs were typically made from templates of porous alumina, polycarbonates or carbon nanotubes through either electrochemical or photochemical processes.(15, 16) Now, GNRs are readily available from a large number of commercial sources and specific sizes or coatings can be requested such as thiol-terminated polyethylene glycol. However, commercial GNRs can vary in the amount of spherical impurities they contain. They are also quite expensive and are not offered at particularly high concentrations. The ability to synthesize GNRs in the lab and functionalize them at high concentrations is crucial to the goals of this work. At a high enough number density, rod-like materials tend to align along their longitudinal axis. The prospect of creating a self-assembled optical metamaterial, then, hinges on being able to produce high concentrations of pure rods at high aspect ratios. (15, 16) With this goal in mind, current methods in literature were

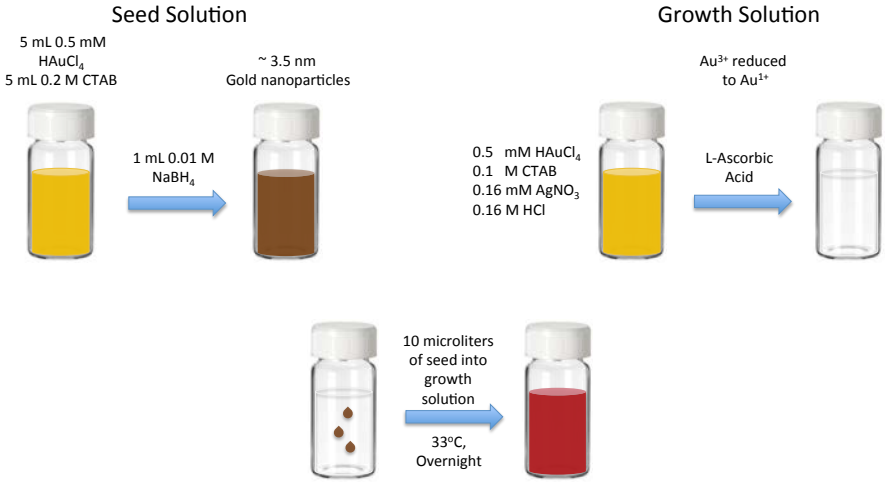

Figure 3.1.1: Typical small batch seed-mediated GNR synthesis. Seed crystals are made by reducing gold (III) chloride with a dilute solution of $NaBH_4$. Separately, a growth solution of Au^{3+} ions is reduced to a clear solution of Au^{+} ions with a weak reducing agent. A small volume of seed crystals is added to the growth solution and left to react overnight.

researched and a variety of groups who have developed useful synthesis procedures were identified.

In 2001, a seed-mediated surfactant-based method was developed by Murphy *et al.*(15, 16) and expanded upon in 2003 by El-Sayed *et al.* (17) This so-called "seed-mediated" approach has been a popular synthesis method ever since because of its simplicity and versatility with no template required. Following this approach, seed crystals are first prepared by reducing an aqueous solution of a $HAuCl_4$ with sodium borohydride. A small amount of seed solution is added to a separate solution of gold (I) ions produced by reducing gold (III) ions with ascorbic acid. Figure 3.1.1 shows a typical seed-mediated GNR synthesis scheme. Almost all seed-mediated approaches utilize aqueous solutions of a stabilizing surfactant, cetyltrimethylammonium bromide

(CTAB), and Ag^+ ions as a template for crystal growth. While the mechanism is not fully understood, it is believed that CTAB along with Ag^+ ions preferentially bind to the {110} facets of the growing gold nanocrystals with the predominate growth along the {100} facet, giving rise to anisotropic rod-shaped growth.(17)

Although the process may seem simple in principle, the formation of high yield, monodisperse high aspect ratio GNRs proved to be very challenging. The purity of rods produced is sensitive to temperature, pH, and final concentrations of reactants. Especially important is the concentration of $NaBH_4$ used when making the seed solution. The presence of too many seed crystals can lead to many sphere shaped deformities. Considerable effort in this work was focused on synthesizing pure, monodisperse rods having varied but well-defined aspect ratios. Early efforts in small batch nanorod synthesis will be presented and compared to results from large batch syntheses and illustrateis dramatic differences in purity. After nanorod synthesis, the functionalization of GNRs will be discussed. The use of a thiol-containing block copolymer, that both solubilizes GNRs in organic solvents and contains functionality for attaching nonlinear organic chromophores, is explored.

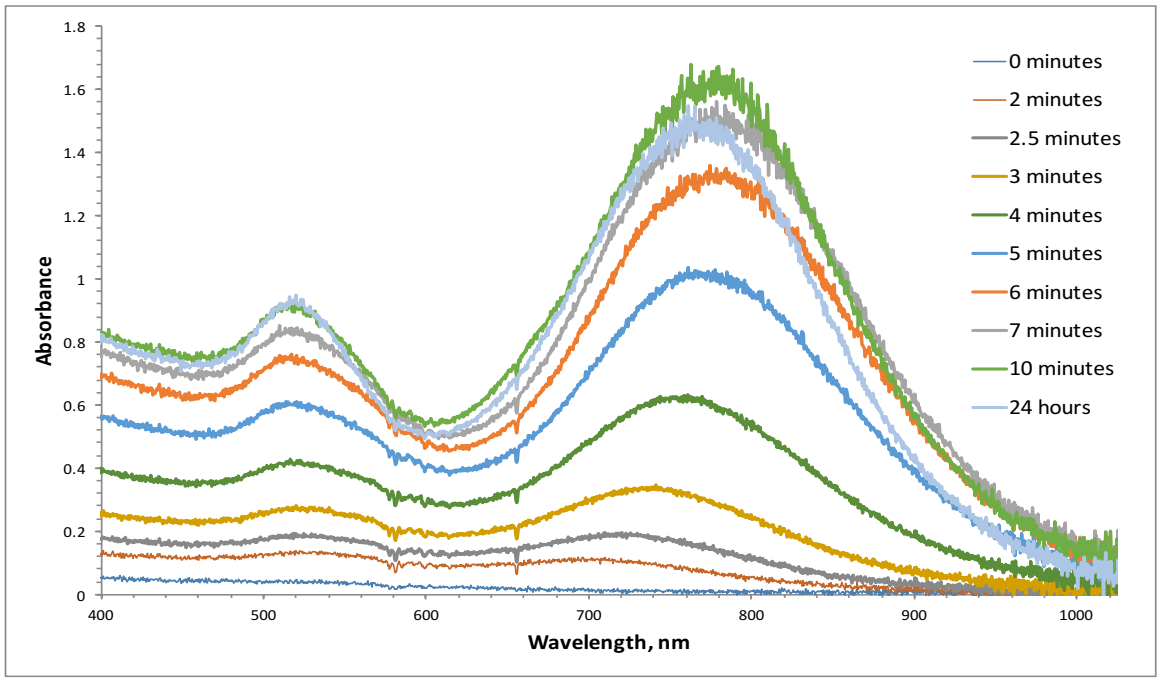

Figure 3.1.2: Absorption spectra of gold nanorod growth over time. These GNRs were synthesized using the basic small batch method shown in Figure 4.1. Growth typically ends after ten minutes.

3.2 – Gold Nanorod Synthesis: The basic synthesis is depicted in figure 3.1.1 and shows the typical components of the seed-mediated method. This unmodified small batch procedure produces nanorods very quickly. Figure 3.1.2 shows the absorption spectra over time of a small batch of GNRs. Growth tends to end at around ten minutes, and many unwanted spherical particles are present indicated by the large absorption near 500 nanometers. When GNRs and other noble metal nanoparticles are exposed to light, the oscillating electromagnetic field induces a resulting oscillation of free electrons in the

metal. A maximum in the magnitude of this oscillation occurs at a frequency known as the surface plasmon resonance (SPR) of the particle. GNRs of certain sizes absorb visible light very strongly and exhibit two distinct SPR peaks called the transverse SPR (TSPR) and longitudinal SPR (LSPR). These two peaks make up the distinctive UV/Vis spectra of GNRs. The weak TSPR peak is always found close to 500 nm along with the SPR of spherical impurities.

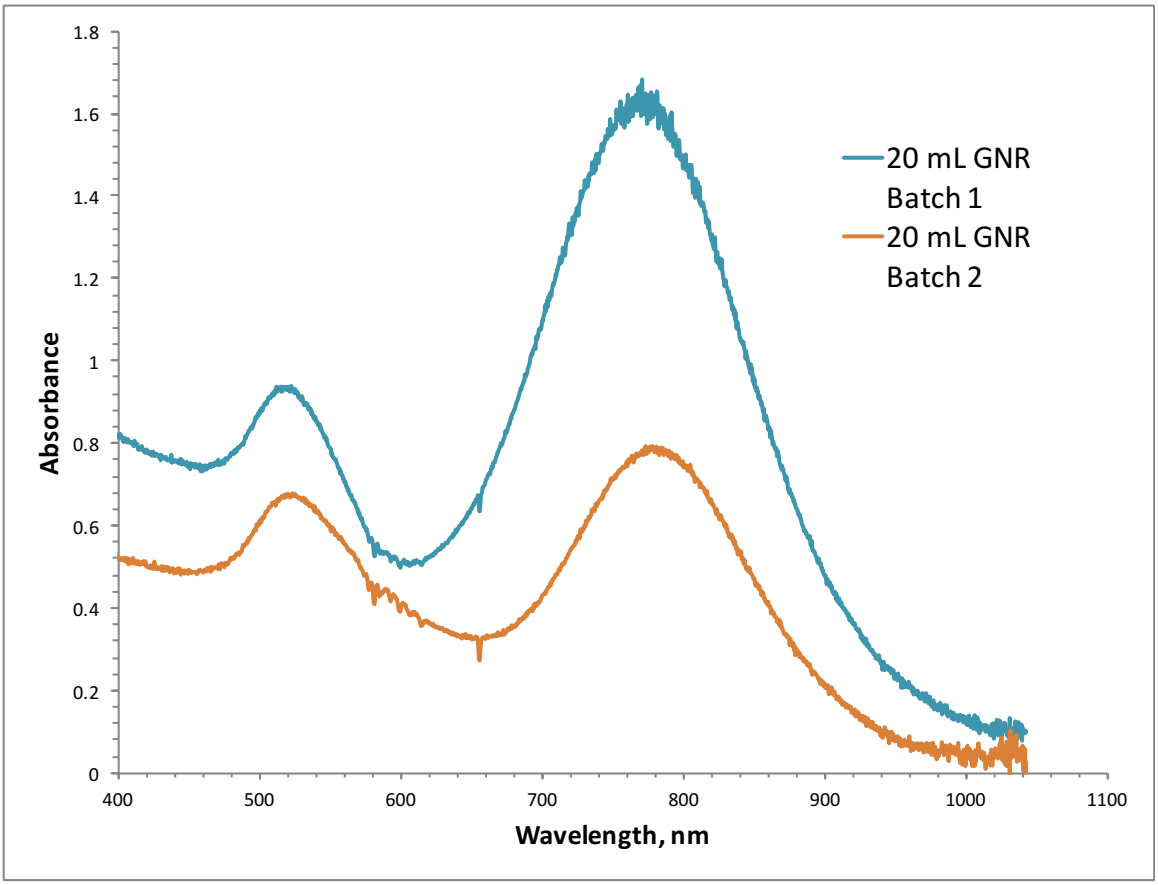

Figure 3.1.3: UV/Vis absorption spectra of two early batches of GNRs at a 20 mL scale. Both of these batches have large amounts of spherical impurities as illustrated by strong absorbance near 500 nm. A highly pure batch of GNRs would have a large ratio of LSPR to TSPR absorbance.

The ratio of rods to impurities can be estimated by comparing the intensity of the LSPR to the peak found near 500 nm. Figure 3.1.3 shows the absorption spectra of two small volume GNR batches with varying amounts of spherical impurities. These small batches were synthesized using a very basic procedure where only ascorbic acid is used to reduce gold (I) ions to gold (0). Typical seed-mediated synthesis uses 10% molar excess of ascorbic acid compared to gold chloride concentration. Using more than this amount of ascorbic acid leads to more spherical particles. According to Vigdermen *et al.*,(18) this result may be due to an increased reduction rate

resulting and an increase of random nucleation events in the growth solution. Ye et al.(19) improved rod synthesis using aromatic additives that slowly reduced Au(III) to Au(0). Compounds such as 5-bromosalicylic acid and sodium oleate were found to offer slow reduction of gold ions. Ascorbic acid was still needed for successful rod formation but at a much lower concentration. Vigderman *et al.* were able to synthesize rods by replacing ascorbic acid with hydroquinone as the reducing agent. Importantly, the conversion of gold ions to rods was found to be near quantitative compared to a 15% conversion typical of more common seed mediated syntheses. These new findings led us to believe that using additional additives had the potential to provide GNRs at higher purities. The following section discusses efforts towards this end.

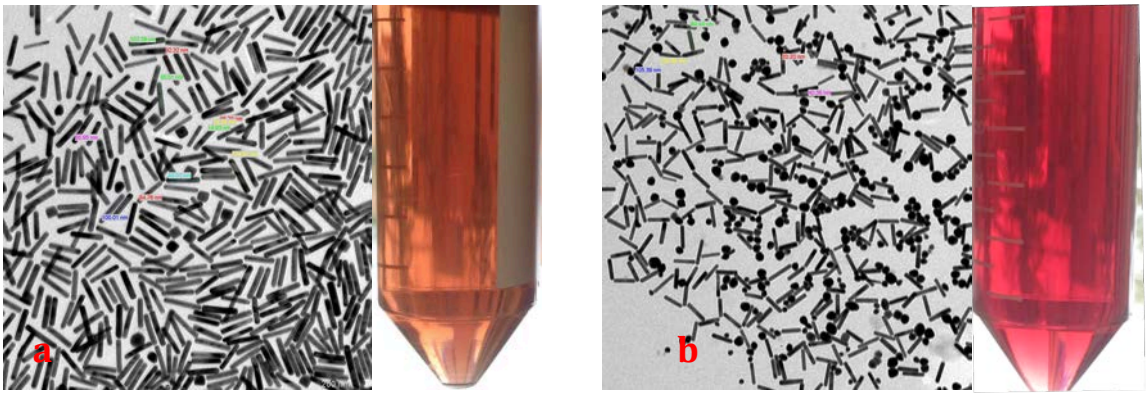

Figure 3.2.1: a) TEM image and photo of nearly monodisperse GNRs from synthesis conditions of Ye et al.(19) b) TEM image and photo of GNRs of similar size but with more spherical particles. Color difference is due to spherical impurities, not due to rod size difference.

3.2 – Gold Nanorod Synthesis Modified to Use Reductive additives: The most recent procedure modified from Ye *et al*.,(19) produces dramatic improvements in the yield of high aspect ratio rods. The improved procedure relies on the use of an additional surfactant: oleic acid. Oleic acid acts as a very mild reducing agent and replaces much of the ascorbic acid used in previous procedures. Less CTAB is needed as well, leading to the belief that the oleic acid also acts as a growth template in tandem with the CTAB. A slow and mild reduction of Au^{+} ions appears to be an important factor in the suppression of spherical impurities. Figure 3.2.1 shows the drastic color difference in solutions of pure rods and solutions containing many spherical impurities. The red hue in figure 3.2.1b illustrates the characteristic color of increased absorbance near 500 nm due to the presence of spherical impurities. Besides using oleic acid as an additive, this improved method allows rod preparation at a much larger 500 mL scale. This has the added benefit of producing more GNRs per batch and being less sensitive to fluctuations in reagent concentration between batches. Generally, GNR synthesis procedures include specific instructions to use ultra pure water, fresh solutions, and aqua regia-cleaned glassware. These precautions were taken at first but it was found that low impurity GNR batches could be produced without the need for such rigorous conditions.

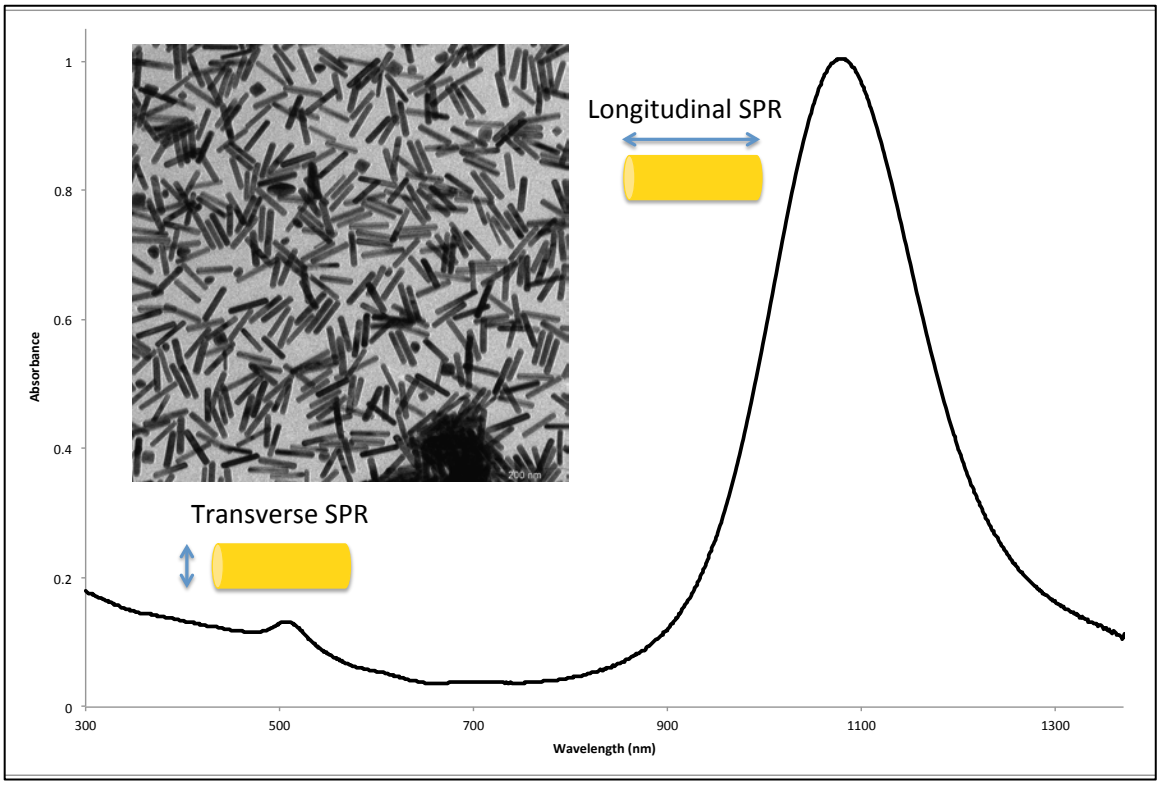

Figure 3.2.2: UV/Vis absorption spectrum of a sample of nearly monodisperse nanorods with aspect ratios of 6-7. Top left inset - TEM image showing small amount of spherical and cube shaped impurities.

Figure 3.2.2 shows the absorption spectrum and resultant transmission electron micrograph of a typical batch of GNRs with a low amount of spherical impurities. Fresh ascorbic acid and sodium borohydride solutions were made and used for each batch while stock solutions of silver nitrate and gold chloride were kept at 0 ºC for weeks at a time before use. Although this method seems to be less sensitive to concentration fluctuations, we were not able to produce high-purity batches until a single critical detail was resolved. In the procedure from Ye's paper, the growth solution is produced by adding an aqueous solution of gold chloride to varying amounts of CTAB, sodium oleate and silver nitrate. We found that after the addition of gold chloride, enough time must be allowed for the sodium oleate to reduce the gold (III) ions to gold (I) ions. The solution starts as a pale yellow and eventually loses all color only after stirring for at least 45 minutes. This observation was not intuitive at because ascorbic acid is typically thought to be solely responsible for this reduction step. Further confusing was the observation that Ye's method still calls for ascorbic acid and indeed, does not successfully produce GNRs without it. After the essential need for ample reaction time was discovered, our modification of this method became very reproducible and a variety of GNRs, having controllably varied aspect ratios (and correspondingly tunable spectra), were accessed.

In an effort to find more efficient synthesis methods, Ye's method was compared to Vigdermen's where hydroquinone replaced ascorbic acid as the mild reducing agent. This method uses a large excess of hydroquinone

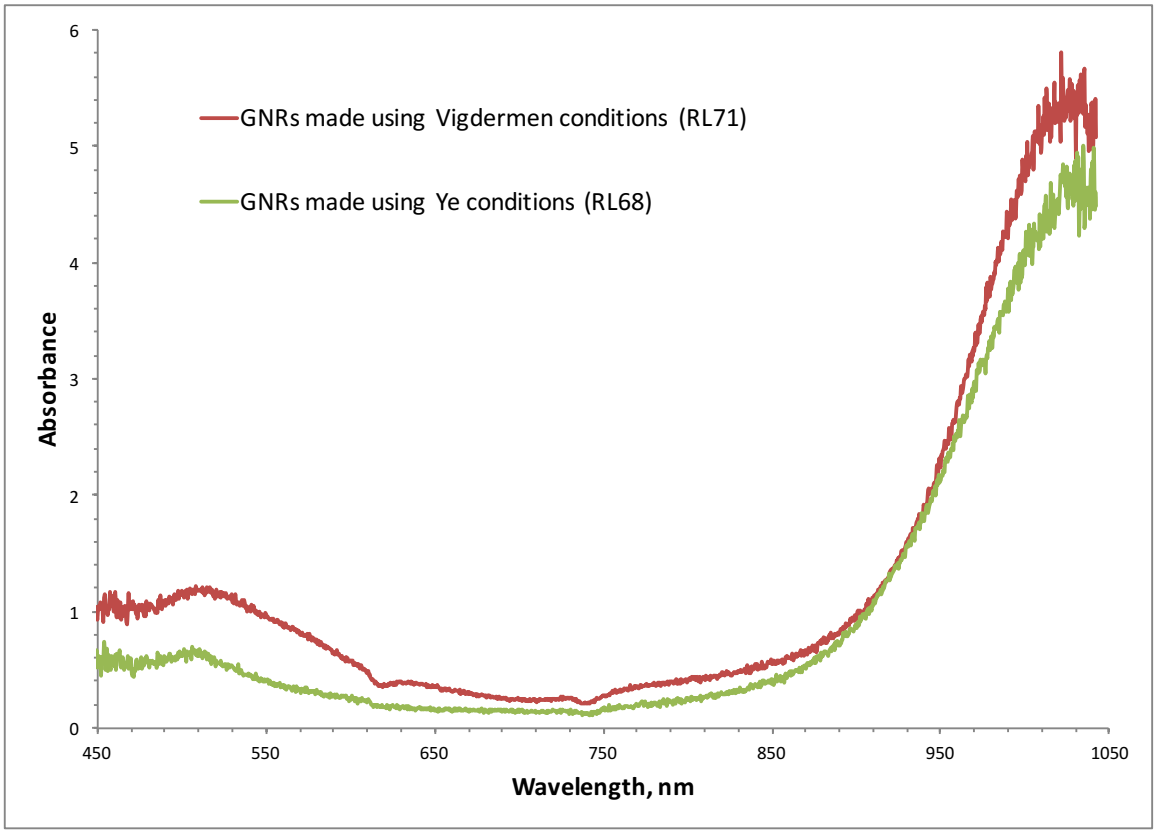

Figure 3.2.2: Absorption spectra of GNRs synthesized using Ye and Vigdermen conditions. Both batches were diluted by the same volume before obtaining absorption spectra. Vigdermen's method did not produce a drastically higher concentration of GNRs compared to Ye's method.

relative to gold concentration that makes fluctuations in concentration less damaging to overall yield and accuracy. Figure 4.6 includes the absorption spectra of two batches of GNRs made with Ye's method vs one made with Vigdermen's. Despite the advantages to using hydroquinone, we determined that Ye's method produced a similar concentration of GNRs. Because Ye's method was reproduced without difficulty at a 500 ml scale, his conditions were chosen for future experiments.

3.3 – Functionalization of Gold Nanorods with Thiol-Containing Block Copolymers: Because an aqueous, seed-mediated method of GNR synthesis was used, the resulting GNRs are coated in a charged surfactant and are not suitable for direct incorporation into polymer films or for the introduction of nonlinear organic dyes. In order to solubilize the GNRs in organic solvents, the use of a thiol-containing block copolymer (see section 2), which both solubilizes GNRs in organic solvents and contains functionality for attaching

nonlinear organic chromophores was proposed. A relatively simple two-step process(9) was investigated and modified for use here in which thiol-terminated polyethylene glycol (PEG-SH) is used to replace the CTAB surfactant already present in aqueous solution post-synthesis. The resultant PEG-SH coated GNRs can be dispersed in an organic solution consisting of a high concentration of custom made thiol-containing polymer. The solution of new polymer competes for the gold surface and replaces the PEG-SH. The resulting product is stable in organic solvents and also contains any functionality included in the design of the thiol-containing polymer.

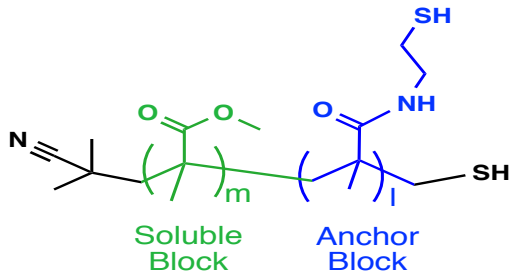

Figure 3.3.1: Gold reactive diblock co-polymer (see section 2).

In order to develop repeatable and effective methods to functionalize GNRs at high concentrations, a simple polymer was synthesized that consisted of a poly(methyl methacrylate) block and a thiol-containing block. The synthesis of this polymer was discussed in section 2 and is illustrated in Figure 3.3.1, with a general depiction of the processes shown in Figure 4.8. The methods of Thierry *et al.*(9) were used as a starting point but modified to adapt the method to higher concentrations of GNRs.

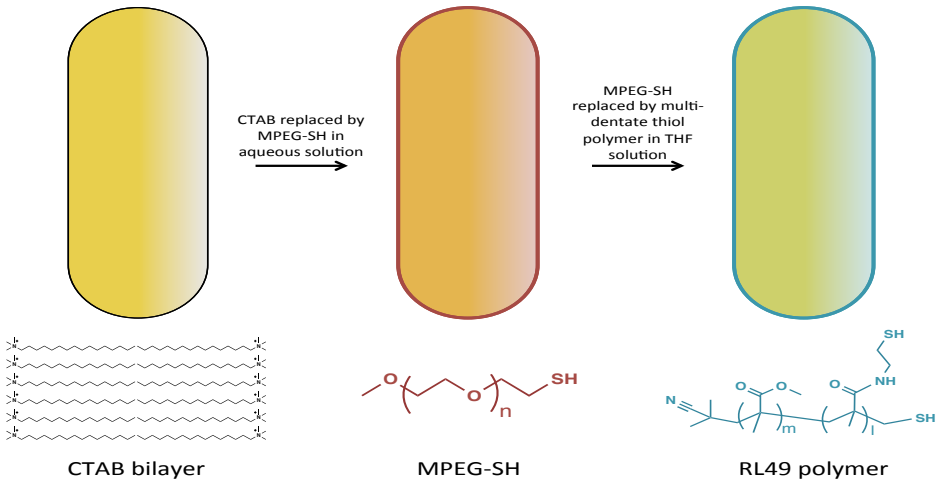

Figure 3.3.2: Overview of GNR functionalization. The CTAB bilayer is first replaced by MPEG-SH, a water-soluble polymer. MPEG-SH GNRs are then soluble in THF and are functionalized with a multi-dentate thiol-containing polymer.

After GNRs are synthesized, the excess CTAB, sodium oleate and other reactants are removed by centrifugation. A typical GNR batch was prepared at a 500 mL scale. 168 mL were collected in 12 plastic falcon tubes each with a 14 mL capacity. After centrifugation, the supernatant containing undesired reactants was carefully removed and each pellet of GNRs was dispersed in 1 mL of deionized water, centrifuged again and redispersed in a total of 6 mL of water. This highly concentrated solution of GNRs was used

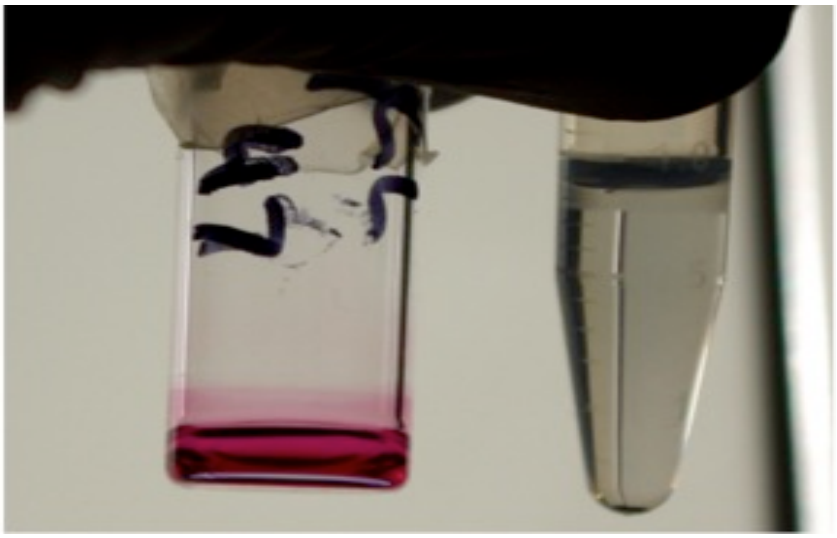

Figure 3.3.3: Left: RL49 polymer-coated GNRs in THF. Right: Unstable CTAB coated GNRs in THF. Loss of color and precipitation occurs immediately after addition of THF.

in the next reaction step without further purification. Additional centrifugation cycles were avoided as any more would reduce the residual CTAB concentration below the threshold for GNR stability. 6 mL of a 1 mg/mL solution of thiol-terminated polyethylene glycol (5000 molecular weight) in water was prepared and added to a 14 mL falcon tube containing 6 mL of highly concentrated GNRs. After brief mixing and sonication, the mixture was allowed to react at room temperature overnight. The literature procedure called for a reaction time of a few hours, however, it was found that an overnight reaction produced GNRs that were stable in organic solvents like tetrahydrofuran much more repeatably. After reacting overnight, the GNRs were purified by centrifugation and could then be redispersed in organic solvents. Although initially stable in organic solvents, PEG-SH coated GNRs were observed to precipitate out of solution after a week at room temperature. Therefore, these THF solutions of GNRs were immediately added to equivolume 5 mg/mL solutions of the multi-dentate thiol-containing polymer shown in figure 3.3.1. After 90 minutes of sonication, the solutions were left to react over night and then purified by centrifugation.

To demonstrate the drastic difference in solubility of GNRs before and after polymer functionalization, a concentrated pellet of CTAB coated GNRs were mixed with THF. Figure 3.3.3 illustrates the obvious insolubility of CTAB-coated GNRs in organic solvents like THF. The GNRs immediately precipitate out of solution as shown by the

dark grey pellet in the bottom of the centrifuge tube. Transmission electron micrograph images were taken of GNRs after functionalization with PEG-SH and the custom thiol-containing polymer. Figure 3.3.4 shows the TEM images of RL68 GNRs after functionalization with PEG-SH and RL49 thiol-polymer. Although the

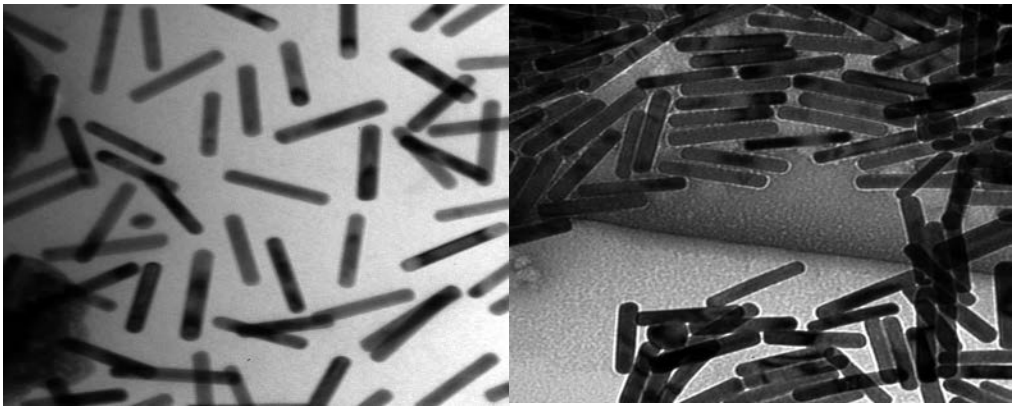

Figure 3.3.4: TEM images of GNRs. Left: Coated in RL49 polymer. Right: Coated in MPEG-SH.

polymer itself cannot be seen in Figure 3.3.4, clearly the GNRs have remained stable and there shape has not been altered after the functionalization process. Solutions of GNRs functionalized with mono-dentate PEG-SH are only stable in organic solvents for approximately one week after which significant precipitation of GNRs is observed.

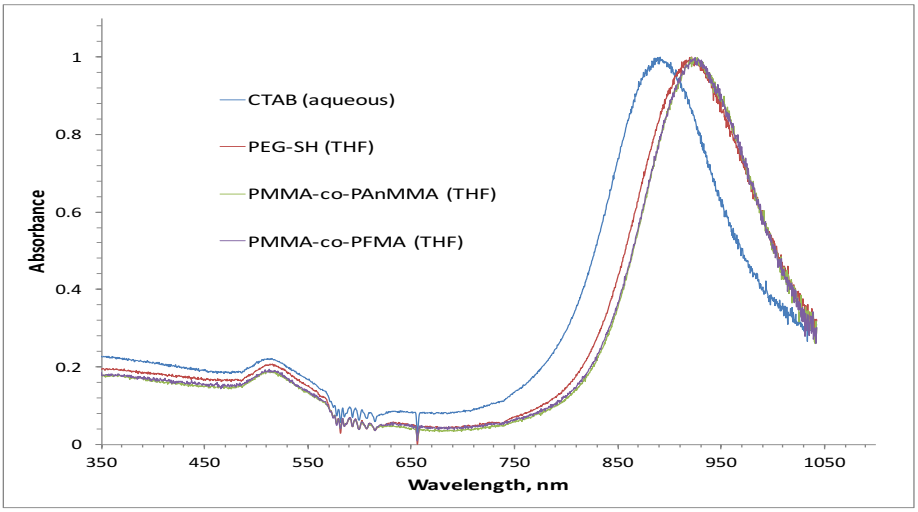

Figure 3.3.5: Absorption spectrum of GNRs in 4 different coatings normalized to the LSPR peak. A red shift in the absorbance of the LSPR peak is observed after replacing MPEG-SH with either PMMA-*co*-PAnMMA or PMMA-*co*-PFMA.

thiol-containing poly(methyl methacrylate-co-furfuryl methacrylate. Figure 3.3.5 shows the normalized absorption spectra of GNRs coated in CTAB, MPEG-SH in THF, and both custom polymers in THF. The distinct TSPR and LSPR absorption peaks are well defined for each coating indicating stable GNRs after functionalization.

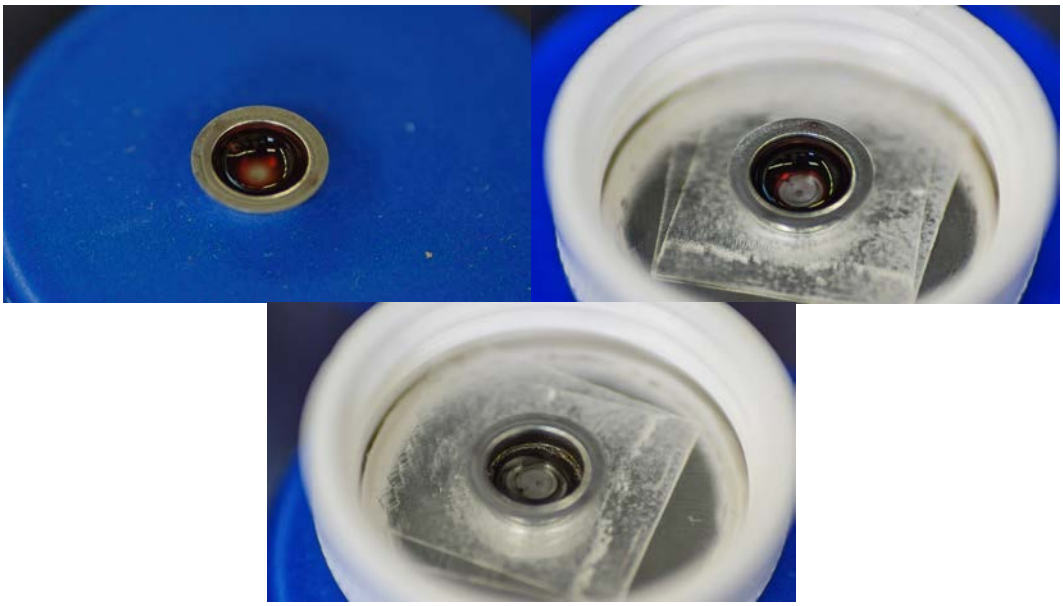

Figure 3.3.6: GNR sample preparation for TGA experiments. GNRs were slowly added in portions to aluminum pans. Solvent was evaporated with nitrogen before further evaporation under vacuum.

Thermogravimetric analysis (TGA) was used to further confirm that our custom polymers were replacing the PEG-SH coating. As GNRs are heated, the compounds adhered to their surface decompose leaving bare gold in the sample pan. The resulting curve shows weight loss percentage versus temperature.

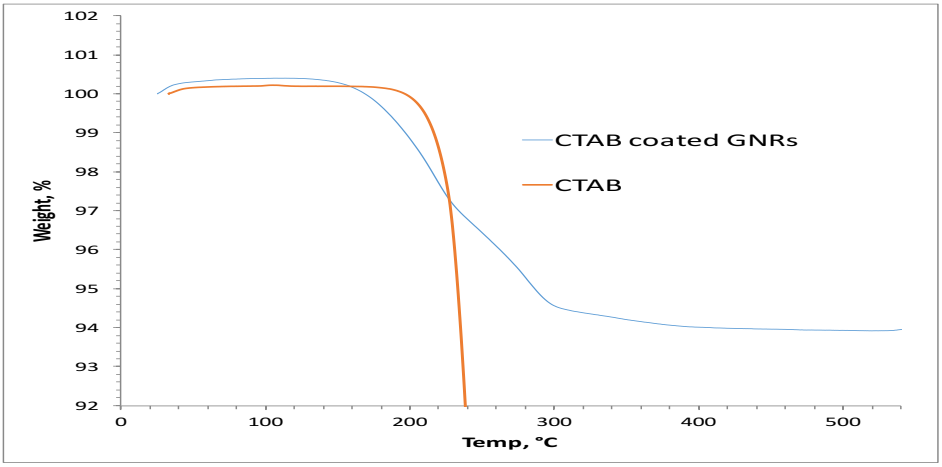

Figure 3.3.7: TGA traces of CTAB coated GNRs and a sample of pure CTAB. The GNR sample begins to lose weight at close to the same temperature of pure CTAB.

Each weight loss profile is unique to the specific surface coating of the GNRs. To prepare samples for TGA experiments, 1 mL of highly concentrated GNRs were centrifuged. The resulting concentrate was redispersed in 50 microliters of solvent before being added slowly in 5-10 microliter portions to an aluminum pan. The solvent (either aqueous or organic) was evaporated by using a flow of nitrogen gas before another portion was added. After the desired portions were added, the pan was placed under vacuum for 1 hour. Using this method, enough GNR weight was added to ensure a successful TGA measurement.

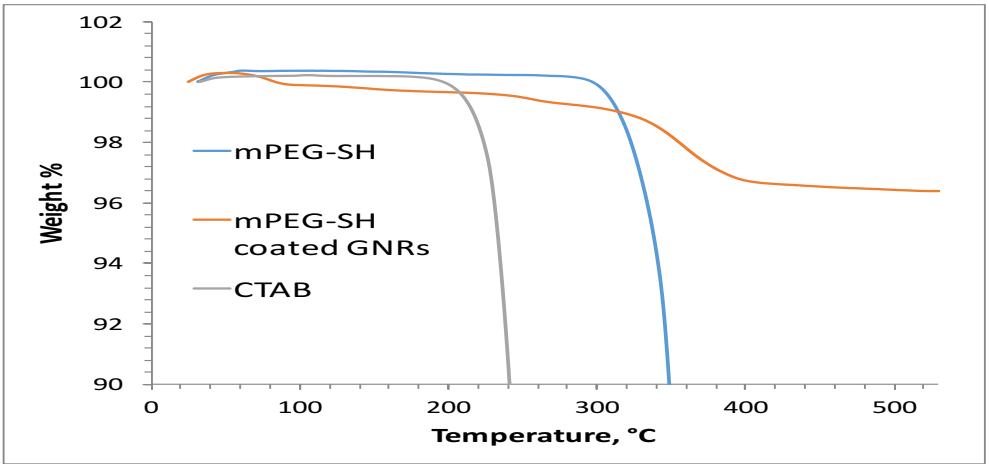

Figure 3.3.8: TGA traces of pure CTAB, pure mPEG-SH and GNRs after reacting with mPEG-SH. Both pure mPEG-SH and GNRs coated in mPEG-SH start losing weight near 350 °C.

GNRs are stabilized in solution by CTAB, during and after synthesis. Weight loss near a similar temperature to that of a sample of pure CTAB is expected. Figure 3.3.7 shows the TGA trace of pure CTAB and GNRs after they have been synthesized.

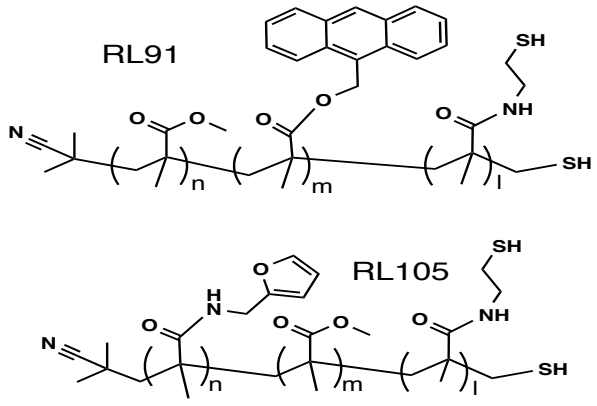

Figure 3.3.9: Structures of polymers used in TGA studies. Both are multi-dentate with respect to gold reactivity and contain Diels-Alder functionality.

Figure 3.3.8 shows a typical TGA trace of GNRs after reacting with mPEG-SH along with traces from pure CTAB and pure mPEG-SH. If any significant amount of CTAB remained on the surface of the GNRs, an obvious weight loss near 200 °C would be observed. An obvious weight loss is observed near 350 °C indicating the GNRs have been functionalized with mPEG-SH. After GNRs were functionalized with mPEG-SH, they were reacted with the polymers found in Figure 3.3.9 as before. TGA was used to determine whether the weight loss profile changed after the reaction took place. Figure 3.3.10 displays the TGA traces of GNRs coated in mPEG-SH and coated in RL91

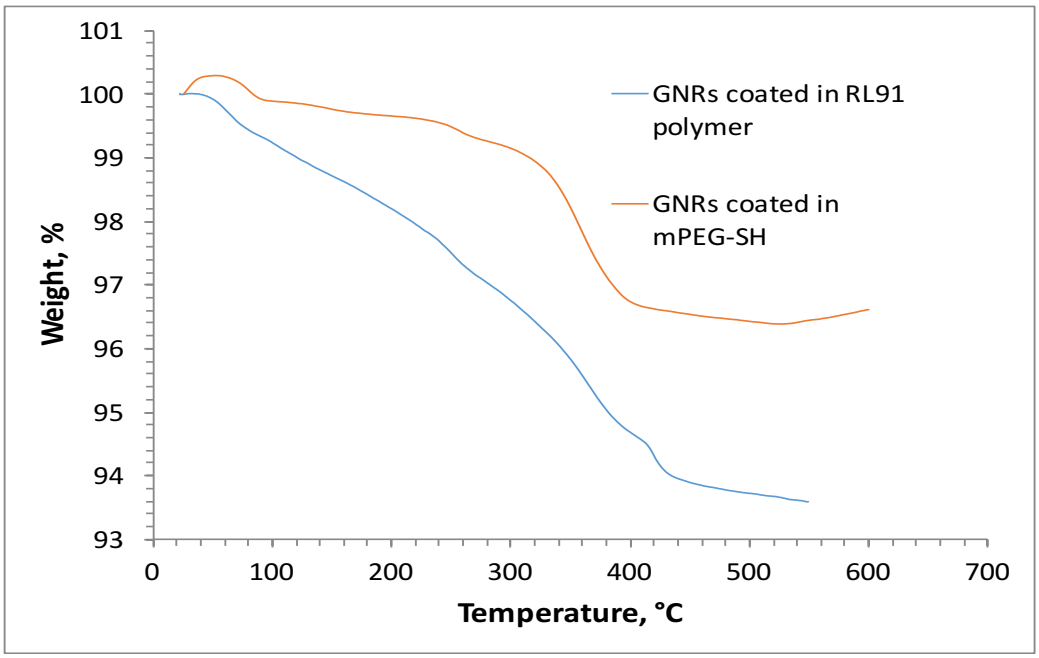

Figure 3.3.10: TGA traces of GNRs coated in mPEG-SH and GNRs coated in RL91 polymer. A distinctive drop in weight near 350 °C is observed for GNRs coated in mPEG-SH but not for GNRs coated in RL91. This indicates that the mPEG-SH has been replaced by RL91.

polymer. A gradual weight loss profile is seen for the sample of GNRs coated in RL91 polymer. The distinctive drop in weight near 350 °C characteristic of mPEG-SH coated GNRs is no longer observed after a reaction with the multi-dentate, furan-containing RL91 polymer. TGA was also used to study GNRs after they reacted with RL105 polymer. When this TGA experiment was performed, the aluminum pan was not tared. Therefore, the weight percent is not corrected for the pan weight. However, the shape of the weight loss curve is still accurate and shows at which temperatures the GNR sample starts to lose weight. Figure 3.3.11 shows the TGA trace for GNRs after they the reaction

with RL105 polymer. The shape is clearly different to that of GNRs coated with mPEG-SH with a gradual loss of weight, more similar to that of GNRs coated in RL91 polymer.

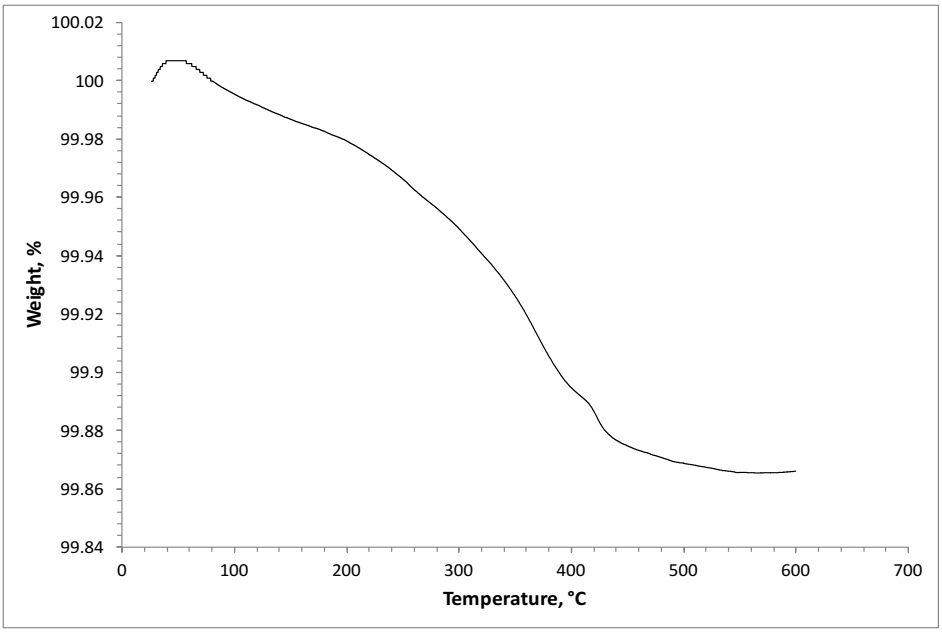

Figure 3.3.11: TGA trace of GNRs coated in RL105 polymer. The weight percent has not been corrected for the tare weight of the pan and sample. However, the shape of the curve still indicates that mPEG-SH has been replaced with RL105 polymer.

3.4 – Preparation of GNR-Doped Polymer Films: After optimizing the procedure for producing organic-soluble GNRs, efforts were turned towards developing a reproducible method for doping polymer films with GNRs. Besides the application toward the main goals of this work, stable films of GNRs have the potential for other interesting technology applications. After discussions with a local technology company, we discovered that the unique absorption profile of GNRs can be useful in the design of new laser materials. Therefore, a collaboration was initiated to test this hypothesis (see section 4). The goal of this additional investigation was to produce a stable UV-curable film of GNRs with tuned absorption specifically at 1064 nm and high transmission at 808 nm. Results of from these studies and their consequences for commercial development are discussed in section 4. In the material presented below, discussion will be limited to early efforts of producing GNR films in commercially available poly(methyl methacrylate-co-ethyl acrylate). This polymer was chosen for its low cost and suitable solubility in common solvents.

To begin the process, RL73 GNRs were functionalized with the thiol-containing polymer previously shown in Figure 3.3.1. Figure 3.4.1 shows the absorption spectra of GNRs throughout the process. A red shift is observed

as the GNRs are transferred from an aqueous environment to an organic environment. After these functionalization steps, various attempts were

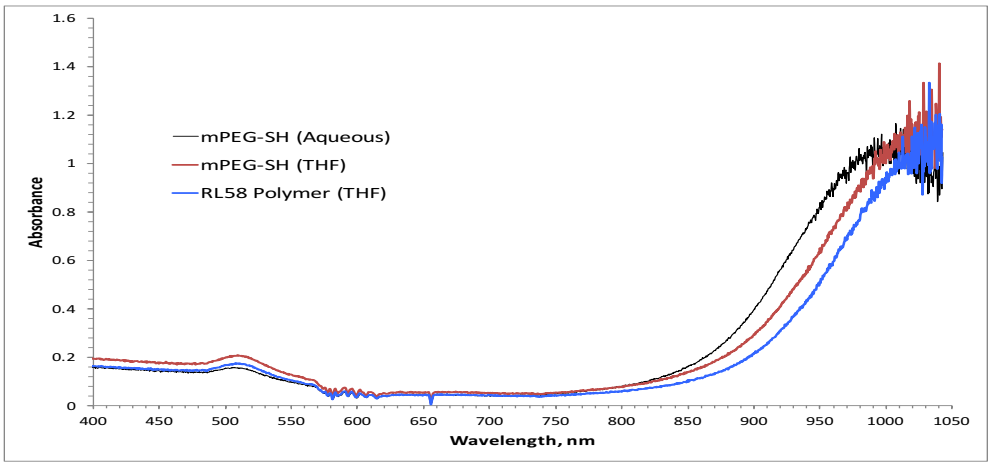

Figure 3.4.1: Absorption spectra of GNRs before doping into polymer films. Labels indicate coating and solvent environment. Although the LSPR peak is cut off, enough is present to suggest GNRs are stable throughout functionalization.

made to dissolve the GNRs into a solution of poly(methyl methacrylate-co-ethyl acrylate) in 1,1,1-trichloroethane (TCE). Because these solutions would be eventually spun on glass slides using a spin coater, the weight percent of polymer in TCE needed to be sufficiently viscous to produce films with a GNR density detectable by UV/Vis spectroscopy. With this requirement in mind, 1.5 mL of GNRs was centrifuged into a concentrated pellet to remove excess solvent. Typically, approximately 300 mg of an 8% weight solution of poly(methyl methacrylate-co-ethyl acrylate) in TCE was added to a GNR

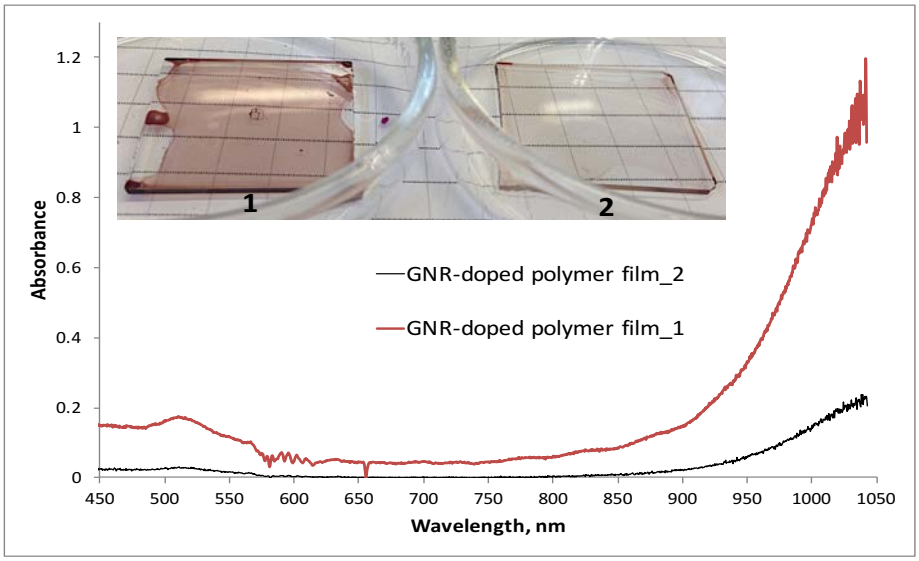

Figure 3.4.2: Absorption spectra of two polymer films doped with different amounts of GNRs.

pellet. After sufficient mixing, the resulting viscous solution was placed on a glass slide and spun using a spin coater. The resulting film was heated at 95°C under vacuum overnight to evaporate solvent. Figure 3.4.3 shows the absorption spectra and photos of two samples of GNRs doped polymer films. The full spectrum is cut off on the long wavelength side due to the limitations of the spectrometer. However, no clouding or precipitation is observed after doping GNRs into polymers and curing overnight. A second, similarly prepared film was heated two more times in order to observe the effects of multiple heating and cooling cycles.

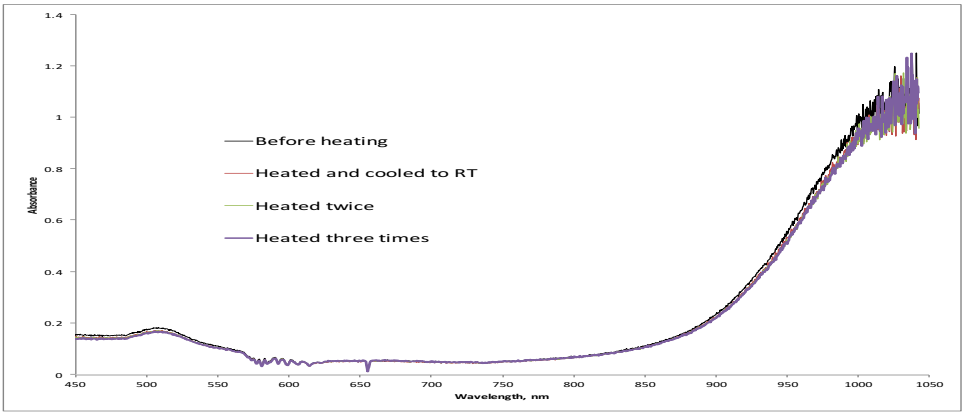

Figure 3.4.3: Absorption spectra of GNR-doped 'film 2' before and after heating multiple times.

Figure 3.4.3 shows the absorption spectra of Film 2 before and after three cycles of heating and cooling. A slight red shift is observed after the first cycle, but no significant change can be seen in the spectra or the appearance of the films themselves.

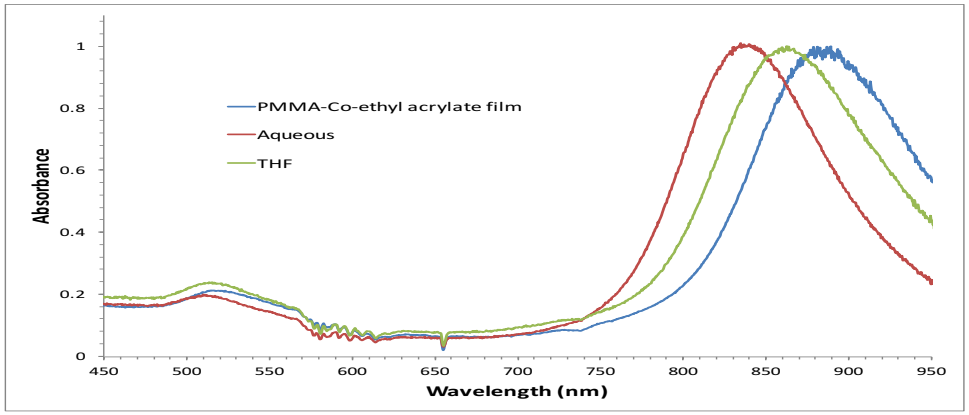

Figure 3.4.4: Absorption spectra of GNRs in water, THF and a thin film of poly(methyl methacrylate-co-ethyl acrylate). Absorption intensity is normalized to the LSPR peak.

In order to observe more of the LSPR peak in the absorption spectra, GNRs of a smaller aspect ratio were synthesized and studied. Figure 3.4.4 shows the normalized absorption spectra comparing the smaller GNRs in water, THF, and a film of poly(methyl methacrylate-co-ethyl acrylate). Importantly, the distinct shape of the LSPR and TSPR peaks are not distorted as the GNRs are moved from their initial aqueous environment. However, a distinct shift in the maximum longitudinal absorption peak can be better observed for the smaller GNRs. The thermal stability of this new GNR film was tested and the polymer coated glass slide was allowed to heat at 95°C for an additional day. Figure 3.4.5 shows the absorption spectra of the GNR film after the first day in the vacuum oven and after one additional day of heating in ambient conditions. Both the distinctive TSPR and LSPR peaks showed no signs of

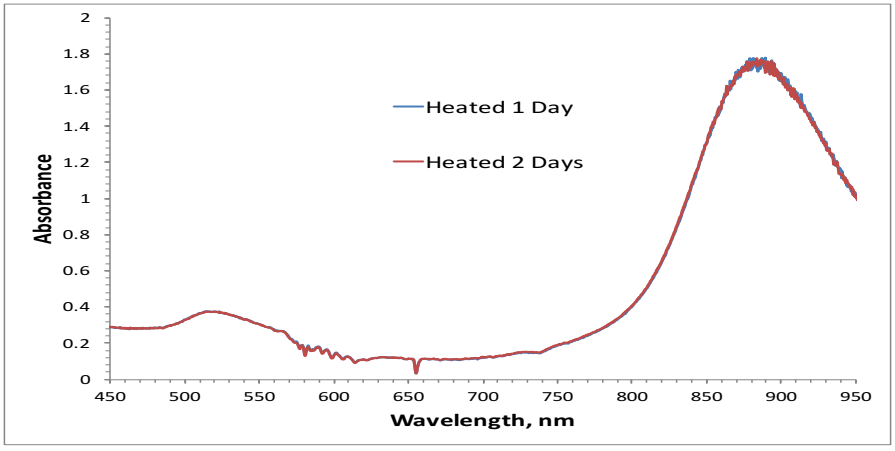

Figure 3.4.5: Absorption spectra of GNRs in a thin film of poly(methyl methacrylate-co-ethyl acrylate) after curing at 95°C for 1 and 2 days. Almost the entire LSPR peak is observed for this sample of smaller GNRs. No shape deformities or shifts in the LSPR peak can be detected.

degradation after heating. This result again shows that GNRs are stable in polymer films, even after heating them to relatively high temperatures.

4) 1064 nm (NIR) Absorbing Gold Nanorod-Doped Epoxy Laser Rod Coating for Improved Laser Efficiency

4.1- Introduction: There are many design parameters to consider when fabricating a laser that operates at high efficiency. Higher efficiency translates into less needed input power, a smaller footprint, and ultimately application to a broader market. When

considering the design of a diode-pumped solid-state laser (DPSSL), the absorption properties of the materials used can significantly affect its efficiency. One of the most common DPSSLs emits at 1064 nm by pumping a neodynium-doped yttrium aluminum garnet (Nd:YAG) rod with an 808 nm diode. Significant emission at 1064 nm occurs laterally out of the laser rod and, when reflected back into the rod by the pump cavity, a depumping phenomenon, amplified spontaneous emission (ASE) occurs.(20, 21) This reduces the efficiency of the laser by stimulating decay from the upper energy level resulting in a lower total level of excited photons occupying that level. This depumping effect can be inhibited by coating the laser rod in a material that is transparent at the pumping wavelength of 808 nm and highly absorptive at the lasing wavelength of 1064 nm. Here it is shown that a Nd:YAG laser rod can be coated with a specially designed gold nanorod-doped epoxy yielding such desirable optical characteristics. This coating allows for absorption and emission at the desired wavelengths with maximum laser output energy increasing by almost two-fold at maximum pump power. Such a coating is easily tunable by chemical means and highly processible. In fact, it can serve as the adhesive that holds the laser rod in place in the cavity assembly, circumventing the need for costly and complex fabrication alternatives (e.g., two-part samarium ceramics) that have been previously explored for this purpose.

DPSSLs are used in many industrial applications, but are not always designed with maximum portability and efficiency in mind. Increased efficiency translates into lower input power and reduces the need for a large power source, accompanied by a heat management system (e.g., water cooling, or thermoelectric). A smaller footprint allows DPSSLs to be used in situations and environments that otherwise would have been impractical. While not the only way to improve laser efficiency, overcoming the aforementioned ASE obstacle hinges on an effective way to coat or enclose the laser rod with a material that is selectively absorptive at one emission wavelength (1064 nm) and transparent at another pump wavelength (808 nm). Currently, one of the common materials used to combat loss of efficiency through ASE is samarium oxide-doped glass or ceramic.(22) However, these materials are difficult to produce and the process of enclosing laser rods requires specialized techniques and equipment. An alternative material that increases laser efficiency while at the same time lowering cost and effort of production would prove very useful.

It was envisioned that a simple epoxy coating acting as a stable absorber would also have the added utility as an adhesive in the laser assembly process. But, the proper additive having all of the necessary physical and optical characteristics is the key to an effective absorptive epoxy coating. Organic molecules (NIR Dyes) that absorb strongly at 1064 nm are known, but tend to be large and complicated to synthesize and may also exhibit significant absorption at 808 nm. Additionally, photo degradation would ultimately render organic NIR dyes unstable and thus, unusable for long-term laser operation. An ideal material would offer ease of synthesis, stability for long-term use, compatibility with commercially available epoxy resins.

Metallic nanoparticles were found to be an intriguing candidate due to their high stability and unique optical properties that depend on size, shape and aspect ratio. Gold nanorods (GNRs) in particular have emerged as popular constructs for optical, sensing, and biomedical applications.(23) As synthesis methods improved, the adoption of GNRs as unique optical absorbers has become widespread. The high density of free electrons on

the surface of GNRs allows for size and shape tunable surface plasmon resonances (SPR). GNRs have two distinct SPR modes: longitudinal and transverse, resulting from their length and width, respectively. The transverse SPR (TSPR) absorbs near 500 nm, while the longitudinal SPR (LSPR) varies depending on the length of the GNR. The advent of simple and efficient solution-based synthesis methods for the preparation of nearly pure GNRs having different lengths permits practical access to absorption profiles in both the visible and near-IR regions of the electromagnetic spectrum. In this work, GNRs were synthesized and functionalized with custom polymers (see sections 2 and 3) in order to produce thermally stable epoxy coatings that absorb at 1064 nm and are transparent at 808 nm with the goal of increasing efficiency, ease of production, and lowering the cost of DPSSLs.

4.2 – GNR Doped Epoxy films as Nd:YAG Laser Rod Coatings: In order to use GNRs in an epoxy coating, pure GNRs at a desired wavelength had to be synthesized and functionalized appropriately**.** The most common method of synthesizing GNRs is the surfactant based seed-mediated method (section 3) GNRs synthesized with this method are only stable in an aqueous environment. Useful methods were therefore developed here to solubilize aqueous solutions of gold nanoparticles in organic solutions by replacing the typical surfactant (CTAB) that stabilizes them in water with organic-soluble alkanethiols. Thiol-terminated polyethylene glycol (PEG-SH) serves as an intermediate stabilization layer that makes the nanoparticles soluble in both water and in organic solvents. The PEG-SH functionalized nanoparticles are then dispersed in a solvent such as tetrahydrofuran and left to react with solutions of a thiol-terminated compound of choice. In this work, gold nanorods were made organic-soluble by using thiol-functionalized copolymers synthesized by the RAFT (Reversible Addition/Fragmentation Chain Transfer) technique. The RAFT polymerization technique was chosen in order to easily access a diblock polymer that provides a highly organic-soluble block, poly(methyl methacylate), and a polydentate anchor block that binds to the GNR surface. The synthesis of the gold-reactive polymer is shown in Figure 2.2.1. Figure 3.3.2 depicts the functionalization process where the GNRs start in an aqueous CTAB environment and end with a mulitdentate thiol-polymer coating. After GNRs are coated in polymer, they can be dissolved in organic solvents like tetrahydrofuran. Organic solutions of GNRs can then be added to solutions of commercial polymers or epoxies and applied to surfaces using casting or spin coating techniques (section 3.4).

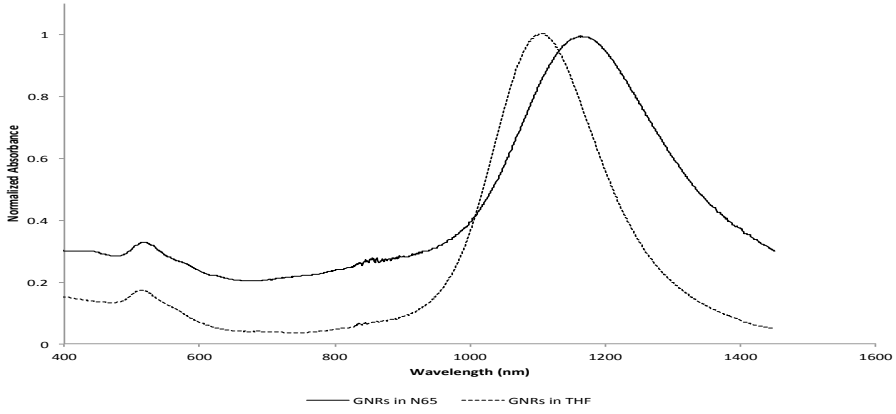

Figure 4.2.1: Absorption spectra of GNRs in THF solution compared to that of a GNR-doped Norland 65 epoxy film, normalized to the LSPR peak.

Figure 4.2.1 shows the absorption spectra of GNRs in Norland 65 epoxy when compared to GNRs in THF. After normalizing with respect to the LSPR peak, a high absorption is still observed at 1064 nm and the distinctive GNR absorption profile is still intact.

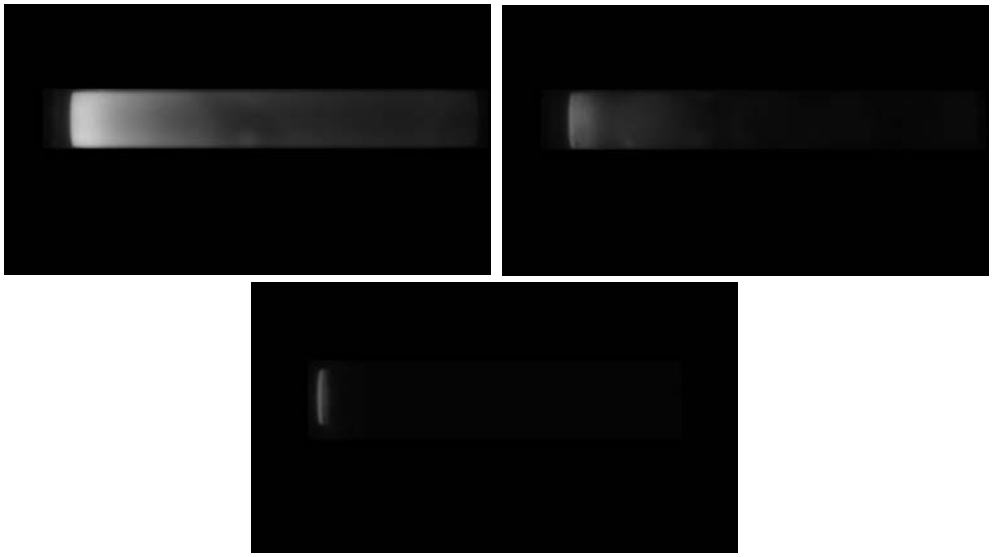

Figure 4.2.2: Fluorescence images at 1064 nm of a Nd:Yag laser rod pumped at 808 nm. Top left: coated in 0.0127 mm of un-doped epoxy. Top right: coated in 0.0127 mm of GNR-doped epoxy. Bottom middle: coated in 0.0254 mm of GNR-doped epoxy. Obvious suppression of 1064 nm fluorescence is observed after coating in GNR-doped epoxy.

In order to simulate the conditions of a production model laser, a Nd:Yag rod was end-pumped at 808 nm with the same laser diode and at the same distance between pump source and laser rod used in a production model. Using an Edmund Optics CMOS camera fitted with a 1064 nm filter, images of 1064 nm fluorescence were obtained perpendicular to the pump direction. Figure 4.2.2 shows the obvious decrease in 1064 nm fluorescence intensity after the laser rod is coated with GNR doped epoxy.

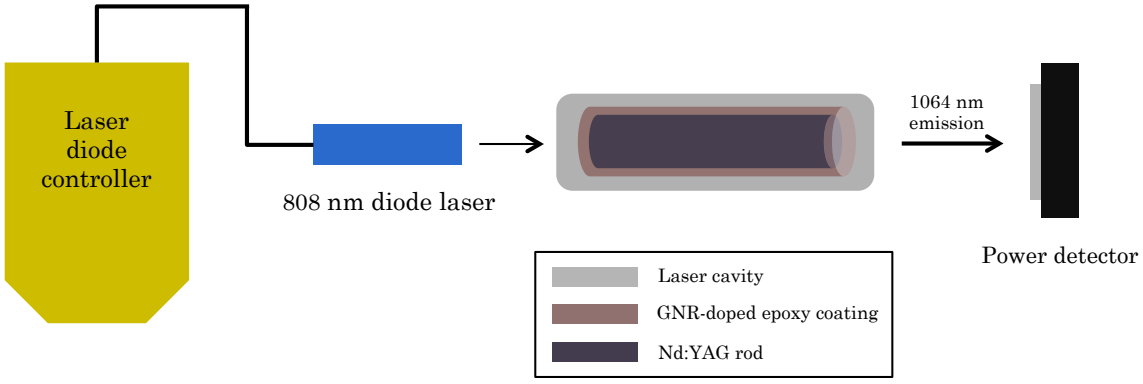

Figure 4.2.3: Schematic illustration of the DPSS Nd:YAG laser constructed for this study.

After the promising fluorescence results were obtained, a functional laser was then constructed (Figure 4.2.3). Following numerous trials, a suitable coating was found that contained 0.015 mL of concentrated GNRs in THF and 0.110 g of epoxy. This coating consistently allowed for absorption of seventy percent of the 1064 nm fluorescence as detected by the camera. After optimizing the coating conditions, the laser components were fully assembled and output efficiency was tested. Figure 5 indicates a significant increase in output energy after the laser rod is coated in GNR doped epoxy. Without a coating, the laser output levels off near 8 mJ. With the GNR coating, the output energy reaches 15.14 mJ.

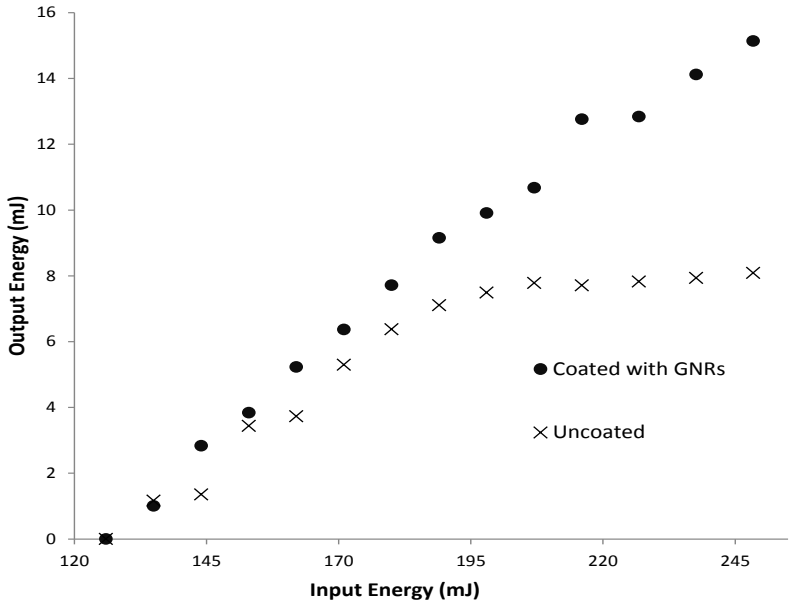

Figure 4.2.4: Laser Efficiency with and without GNR coating. The uncoated rod output energy rolls off in a simple Q-switch resonator due to the increase in ASE losses as the gain is increased. The rolloff in the coated rod has increased significantly allowing more stored energy and greater output energy.

A Quantum Composers (1550 series) laser diode driver controller was used to produce the curve showing output energy vs input energy. A Gentec-EO energy detector (QE12LP-S-MB) was used to detect the output energy.

5) ONLO Functionalized Vertical Gold Nanopillar Samples:

5.1 - Theoretical Analysis of Nonlinear Metamaterials: We have applied computational modeling to explore NLMM design parameter space in order to identify the elements that are most critical to control over local field magnitude, orientation and interaction. In collaboration with the David R. Smith research group, we have adapted recently developed coupled-mode theory(24) based on Bloch mode analysis to investigate a metamaterial structure composed of a nematic-like array of gold nanorods (65 nm length, 8 nm width) interspersed with a uniform nonlinear dielectric.(3) This theoretical analysis is used to relate the effective $\chi^{(2)}$ (second-order nonlinear susceptibility) of the medium to overlap integrals in the limit that the lattice constant is much smaller than a wavelength. The results from this modeling thus far have demonstrated that within such an inhomogeneous (periodic) medium, local fields can vary dramatically from macroscopic and applied fields, both in magnitude and direction. Field concentration (which is quite evident here) for enhanced nonlinear optical effects, has been the dominant motivating factor in the development of nonlinear metamaterials and nonlinear plasmonics.(4) However, significant opportunity also exists to simultaneously gain control over local field directionality. This control over the directionality of internal fields allows access to entirely new properties, fundamentally different in nature than those exhibited by the constitutive materials. More specifically, NLMMs may be designed such that incident waves with orthogonal polarizations, which would not normally display a large degree of overlap, may be highly coupled by resulting local fields.

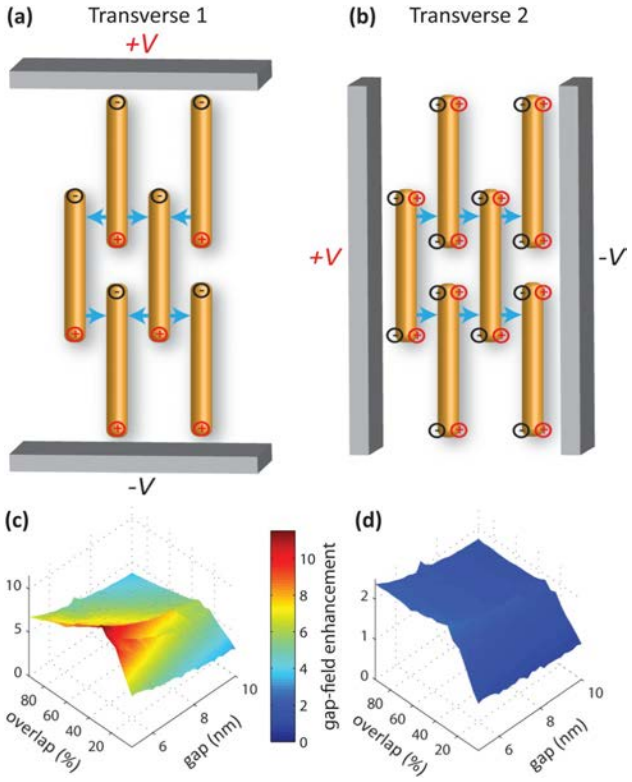

Figure 5.1.1: Schematic of the local fields (a), (b) and estimate of the local field enhancement in the gaps between nanorods (c), (d) for the two transverse electric field polarizations.(3)

In the example shown here (Figure 5.1.1), the nonlinear metamaterial (NLMM) configuration under test consists of an array of metallic (gold) nanorods aligned in a parallel configuration. The simulation parameters assume that the medium interspersed between the nanorods exhibits a nonzero $\chi^{(2)}$. Figure 5.1.1 illustrates the structurally induced local field effects that are computationally predicted for off-resonance operation. Figure 5.1.1c shows that with a rod overlap of ~ 50% and an inter-rod distance of ~ 6 nms, local fields may be enhanced by approximately an order of magnitude. In addition to simple local field enhancements, figure 5.1.1a and 5.1.1b also show that regardless of the directionality (polarization) of the externally applied field, significant local electric fields are induced in the gaps between rods. These local fields are always oriented orthogonally to the rod long axis. It is these local fields that are predicted to give access to improved overlap between orthogonally polarized incident waves. This behavior may be further elucidated by investigating the effect such a structure has on electrooptic modulation (Pockels Effect) efficiency.

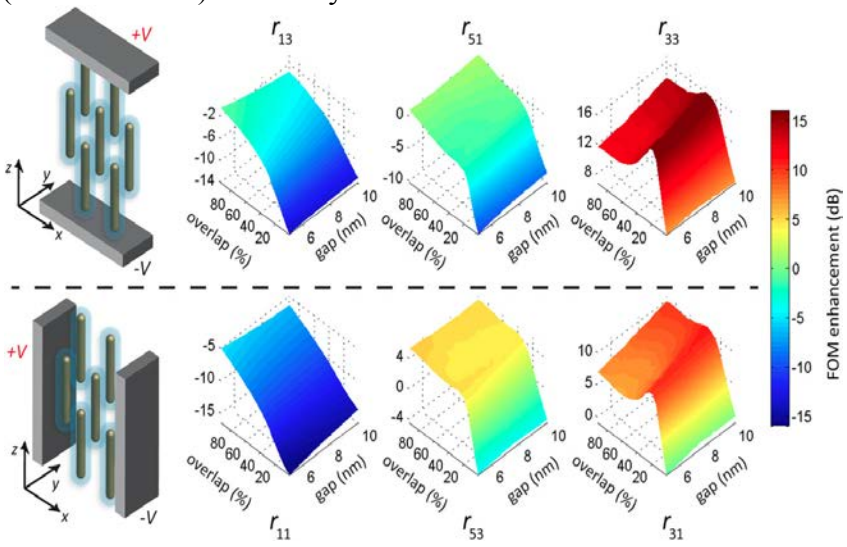

Figure 5.1.2: Magnitude of the Pockels coefficient figures of merit for the gold nanorod-ONLO array. $(n_i n_j)^{3/2} r_{ijk}$ normalized by the figure of merit for the ONLO itself ($n^3 r_{33}$), plotted in dB. The plots are separated by row, corresponding to two electric field configurations, shown schematically: electric field polarized along z (top row) and electric field polarized along x (bottom row).(3)

Figure 5.1.2 illustrates simulations of electrooptic modulation corresponding to the gold nanorod-ONLO array. The product of propagating and DC fields were used to excite the ONLO according to its local nonlinear tensor. The reradiated fields were collected at the entrance and exit planes of the simulation. The nonlinear parameter retrieval method(4) was then applied to analyze the results and calculate the effective bulk nonlinear susceptibility. This process was then repeated for all possible permutations of poling field orientations and propagating wave polarizations. Pockels Effect (r_{ijk}) coefficients were then calculated based on

$$r_{ijk} = \frac{\varepsilon_0^2}{\varepsilon_i \varepsilon_j} \chi_{ijk}^{(2)}$$

These coefficients were finally plotted based on the electrooptic modulation figure of merit $(n_i n_j)^{3/2} r_{ijk}$ normalized against $n^3 r_{33}$.(25) These simulations reveal that, as expected, the coefficeints r_{33} and r_{31} are the largest for either electric field configuration, and can be enhanced by an order of magnitude or more compared to the ONLO alone. These simulations also reveal the presence of significantly strong r_{51} and r_{53}. These coefficients represent the ability of a DC field to induce coupling between the two originally orthogonal polarizations. This differs drastically from a homogeneous medium, which would need to employ an ONLO with a large off-diagonal nonlinear tensor element. Such materials are not readily available.

5.2 - Sum Frequency Generation (SFG) Analysis of ONLO Functionalized Gold Nanopillar Arrays: SFG is a nonlinear optical spectroscopy technique that is frequently used to study layers of molecules bound to surfaces due to the inherent symmetry breaking that occurs at an interface.(26) This technique is related, in principle, to Second Harmonic Generation (SHG) in that a signal is only generated when a nonzero $\chi^{(2)}$ exists. However, in contrast to SHG, SFG occurs when there is sufficient spatial and temporal overlap between two separate incident optical fields to create an output with a frequency (ω) that is equal to the sum of the two input frequencies (equation 5.2.1).

$$I_{SF}(\omega) \propto \left|\chi^{(2)}\right|^2 I_1(\omega_1) I_2(\omega_2) \qquad \text{Eq. 5.2.1}$$

Here the intensity of the output $I_{SF}(\omega)$ is proportional to the square of the first nonlinear susceptibility of the medium under study and the intensities of the two inputs $I_1(\omega_1)$ and $I_2(\omega_2)$. Even when other conditions are satisfied, $I_{SF}(\omega)$ is only nonzero when $\chi^{(2)}$ is nonzero.

The SFG technique is particularly useful for the study of NLMMs because the polarizations of $I_1(\omega_1)$ and $I_2(\omega_2)$ may be altered relative to one another and to the sample, in order to test for the existence of off-diagonal nonlinear tensor elements such as those theoretically predicted in section 4.1 above.

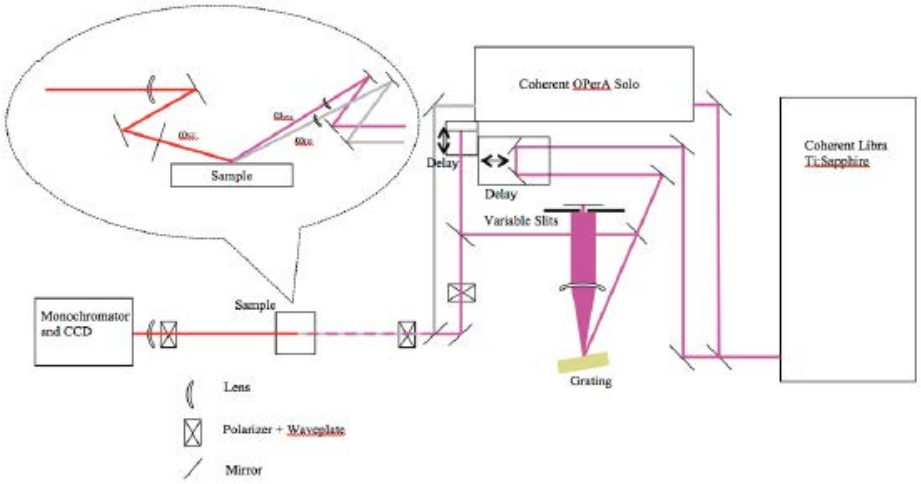

Figure 5.2.1: Schematic of the SFG setup in the Walker Research Lab at MSU.

The SFG setup constructed in the Walker Research Laboratory at Montana State University was used for the experiments described here (Figure 5.2.1). This setup consist of a Ti:Sapphire (Coherent, Libra –HE) laser with a 1kHz repetition rate, 85fs pulse duration, and an average power of 3.9W. This laser produces $I_1(\omega_1)$ = 801nm (visible beam) and is used to pump the OPerA Solo (Coherent) optical parametric amplifier to produce $I_2(\omega_2)$ = 3250nm. Both beams are simultaneously incident on the sample, and a high-sensitivity CCD camera is used to collect $I_{SF}(\omega)$.

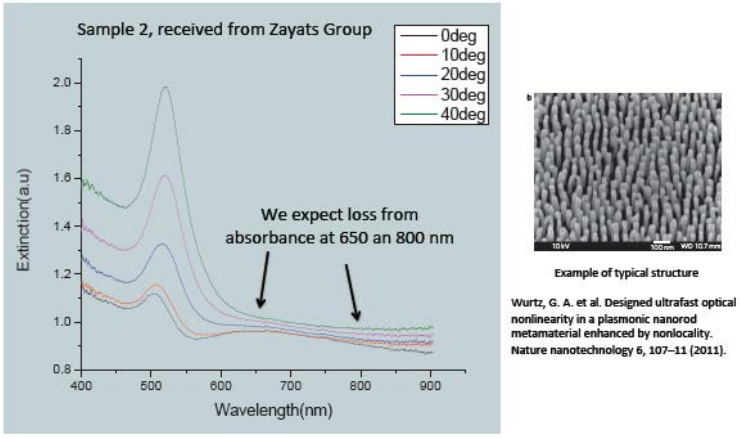

Figure 5.2.2: Scanning Electron Microscope (SEM) image of a gold nanopillar sample (right), Corresponding UV-Vis absorption spectrum at incidence angle intervals decreasing from 90 (Left).

Figure 5.2.2 (right) shows an SEM image of a vertical gold nanopillar sample provided by the Anatoly Zayats Laboratory, London. This sample was prepared by anodization of a smooth aluminum film evaporated on a gold-coated glass slide. Anodization creates a regularly spaced array of nanopores in which gold is then electrodeposited. Following gold deposition, the remaining aluminum oxide layer is removed using a basic wash

solution to yield a vertical gold pillar array.(27) Linear dichroism measurements are shown (figure 5.2.2, left). The absorbance of plane polarized light increases as the angle of incidence decreases from the sample normal, confirming optical anisotropy.

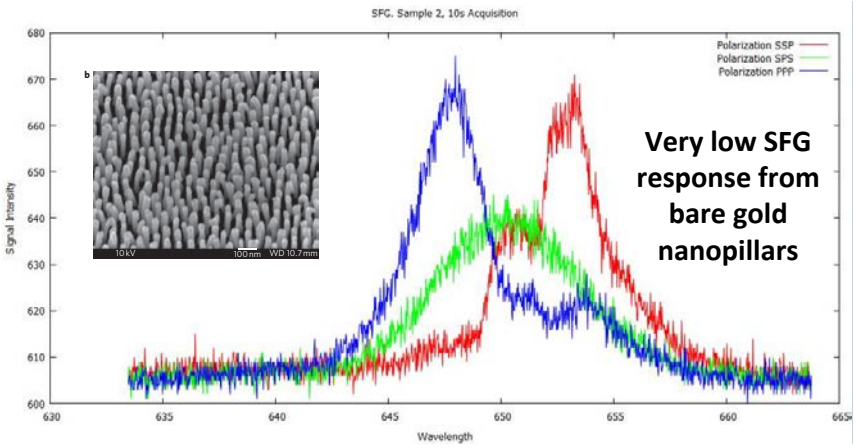

Figure 5.2.3: Preliminary SFG analysis of bare vertical gold nanopillar sample.

Figure 5.2.3 illustrates data resulting from preliminary SFG analysis of bare (no ONLO) vertical gold nanopillar samples. Polarization XXX notation is given as: first letter = polarization of output $I_{SF}(\omega)$; second letter = polarization of 3250nm $I_1(\omega_1)$; third letter = polarization of 801 nm $I_2(\omega_2)$. Thus, Polarization SPS denotes: output polarizer set parallel with the sample surface (S); IR input $I_1(\omega_1)$ set to perpendicular with the sample surface and parallel with the gold nanorod long axis (P); and visible input $I_2(\omega_2)$ set parallel with the sample surface. From inspection of figure 5.2.3, it is tempting to conclude that bare vertical nanorod samples exhibit nonzero $\chi^{(2)}$ and display an interesting response to varied input polarizations. However, $I_{SF}(\omega)$ is quite low and noisy for this sample and care must be taken in analyzing this data.

Scheme 5.2.1: Synthesis of AT ONLO 1 via esterification of ONLO 1 using lipoic acid.

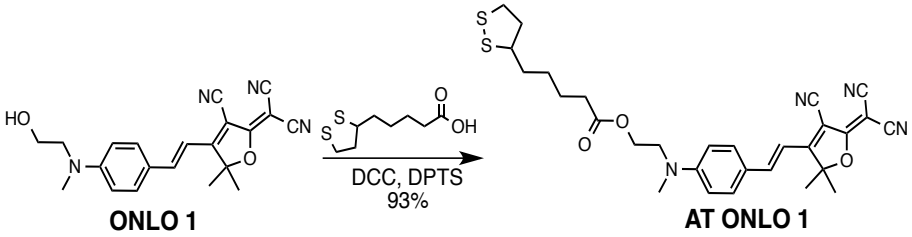

In order to evaluate the effect on SFG response of simply binding an alkane-thiol terminated ONLO to a flat (not nanostructured) gold surface monolayer samples were tested via polarization resolved SFG. ONLO 1 was prepared in the Sullivan Research Lab at MSU, using modified organic synthesis protocols (Scheme 5.2.1). Standard procedures were used to prepare ONLO 1, to which alkane-thiol functionality was added via esterification of the terminal hydroxyl group with lipoic acid.(28) This alkane-thiol

terminus bonds strongly to any clean gold surface, allowing near-covalent strength binding of the desired ONLO.

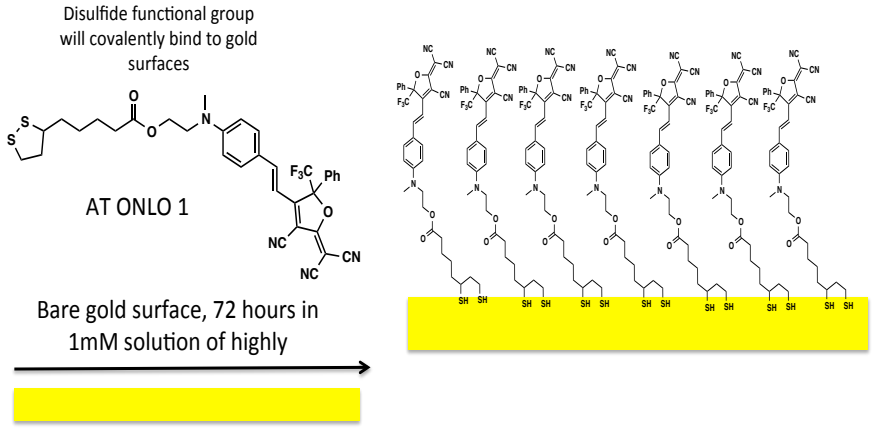

Figure 5.2.4: Schematic illustration of gold surface functionalization with alkane-thiol terminated ONLO (AT ONLO 1).

To prepare AT ONLO 1 functionalized gold films, flat gold on glass was thoroughly cleaned via sonication in absolute ethanol. A 1mM solution in dichloromethane of AT ONLO 1 was then prepared. Each gold film was soaked in the AT ONLO 1 solution for 72 hours before rinsing and drying. Such treatment is known to yield a unidirectional surface monolayer due to gold-thiol bonding (figure 5.2.4). Such a monolayer is $\chi^{(2)}$ active due to the inherent symmetry breaking effect of unidirectional surface attachment.

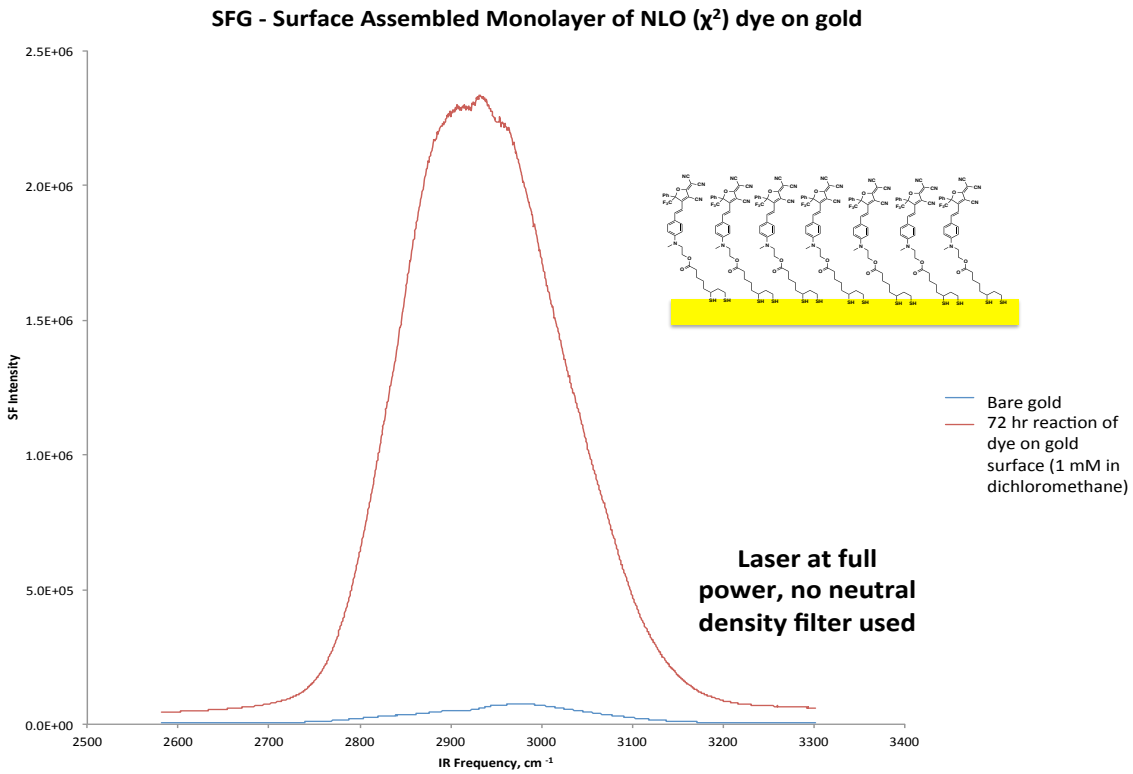

Figure 5.2.5: Comparison of SFG signal from a bare (no ONLO) flat gold surface (blue line) with that from AT ONLO 1 functionalized flat gold film (red line).

The SFG signal, arising from the Polarization PPP configuration, for an AT ONLO 1 functionalized sample (figure 5.2.5: red) shows a ~ 2,000 fold enhancement when compared to bare (no ONLO) flat gold substrate (figure 5.2.5: blue). Our current understanding is that this very large enhancement in SFG intensity may be explained by interaction of the gold film's P polarized surface plasmon resonance (SPR) enhanced electric field with a highly organized $\chi^{(2)}$-active AT ONLO 1 monolayer. Theoretical modeling and further experimentation are currently underway in order to better explain this phenomenon. In order to assess the behavior of the AT ONLO 1 functionalized gold film with respect to orthogonal input polarizations, Polarization SSP and Polarization SPS configurations were examined. These experiments determined that only very weak SFG intensity is observed for any polarization configuration other than PPP. Such a result suggests that, as may be expected, orthogonal input polarizations do not interact well due to the lack of a strong off-diagonal $\chi^{(2)}$ tensor element.

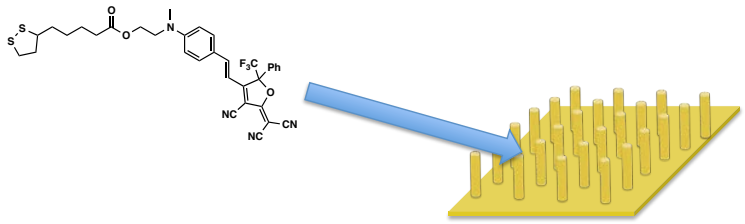

Figure 5.2.6: Preparation of AT ONLO 1 functionalized vertical nanorod (nanopillar) arrays. Conditions used to prepare AT ONLO 1 functionalized flat gold films were duplicated.

Preparation of AT ONLO 1 functionalized nanopillar samples proceeded by essentially duplicating the conditions used for the preparation of AT ONLO 1 functionalized flat gold surfaces. A 1mM solution of AT ONLO 1 in dichloromethane was prepared. Nanopillar samples provided by Anatoly Zayats were then cleaned absolute ethanol and soaked in the AT ONLO 1 solution for 72 hours. The samples were then rinsed thoroughly and dried in air.

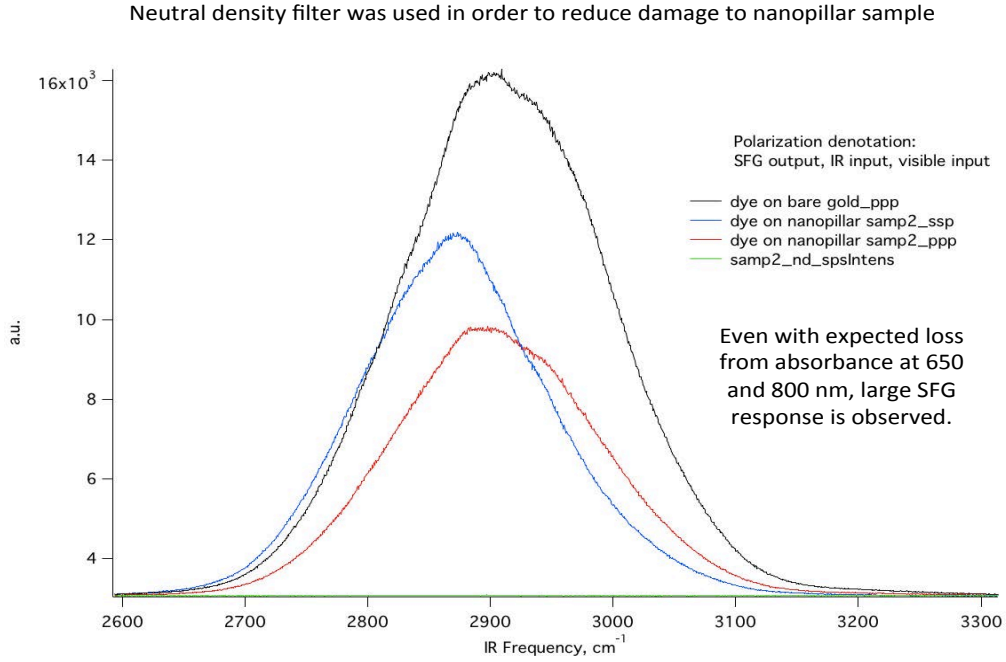

Figure 5.2.7: Nanopillar samples functionalized with AT ONLO 1 analyzed using polarization resolved SFG spectroscopy compared against AT ONLO 1 functionalized flat gold sample (black line). Polarization configurations: PPP (red line); SSP (blue line); and SPS (green line) are shown.

Polarization resolved SFG spectroscopy was again used to analyze the AT ONLO 1 functionalized nanopillar samples. Representative results are illustrated in figure 5.2.7.

Polarization PPP configuration signals are plotted for the AT ONLO 1 functionalized nanopillars and for AT ONLO 1 flat gold surfaces for comparison. Inspection of the figure shows that the Polarization PPP SFG signal is still very strong for the nanopillar sample although it appears to be somewhat attenuated compared to the flat gold surface. Analysis of these results is currently ongoing, but it must be noted that the bare nanopillar sample absorbs strongly at both $I_1(\omega_1)$ = 801 nm and $I_{SF}(\omega)$ ~ 650 nm potentially leading to an artificial appearance of signal attenuation. In contrast to the AT ONLO 1 functionalized flat gold surface, the AT ONLO 1 nanopillar sample also shows strong SFG in the Polariztion SSP configuration (figure 5.2.7: blue line). This suggests the existence of a large off-diagonal $\chi^{(2)}$ tensor element, consistent with our theoretical predictions. This is potentially a very significant result because it appears to confirm that nanostructured hybrid metallic nanostructure/ONLO NLMMS may indeed allow enhancement and control of nonlinear optical effects useful for a myriad of applications. Further testing is currently underway and will be continued through funding period 3. A publication detailing these results is currently in preparation.

5.3 – Future work on ONLO Functionalized Gold Nanopilar Arrays: In collaboration with Professors Zayats, Walker, and Smith, we plan to continue our work on the nonlinear optical properties of ONLO Functionalized Gold Nanopillar Arrays. In particular we plan to: 1) Use multi-scale theoretical analysis to help analyze current results and to provide useful property predictions; 2) Prepare new alkane-thiol functionalized ONLOs with varied spectral properties so that we may tune the observed nonlinear optical response; 3) Work with Professor Anatoly Zayats to prepare nanopillar samples with tuned spectral properties.

Scheme 5.3.1: Schematic illustration of the synthesis of ONLO 1 and 2. ONLO 1 was found to have an optical absorption maximum of λ_{max} = 550 nms whereas for ONLO 2 λ_{max} = 600 nms

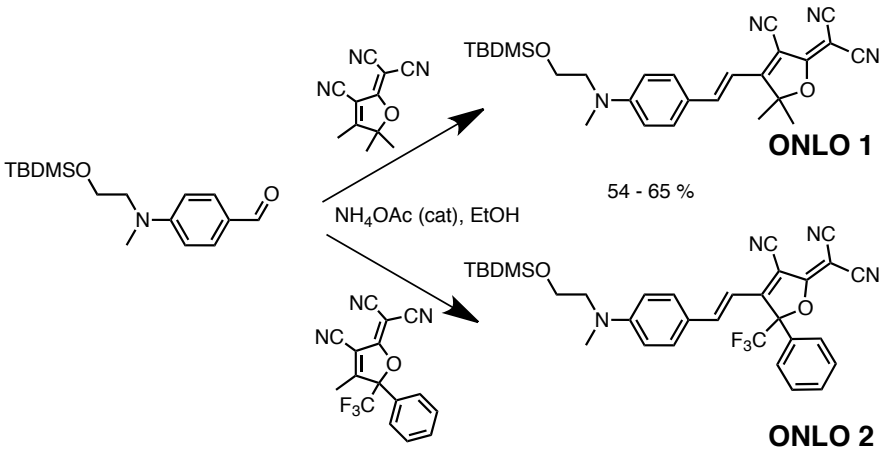

As an example, scheme 5.3.1 illustrated the synthesis of ONLO 2, which may be used in an analogous manner to that shown in scheme 5.2.1 to prepare AT ONLO 2. AT ONLO 2

will be bathochromically shifted compared to AT ONLO 1, and will help to elucidate ONLO and nanopillar sample behavior. The absorption spectra corresponding to ONLO 1 and ONLO 2 are shown for comparison in figure 5.3.1 below.

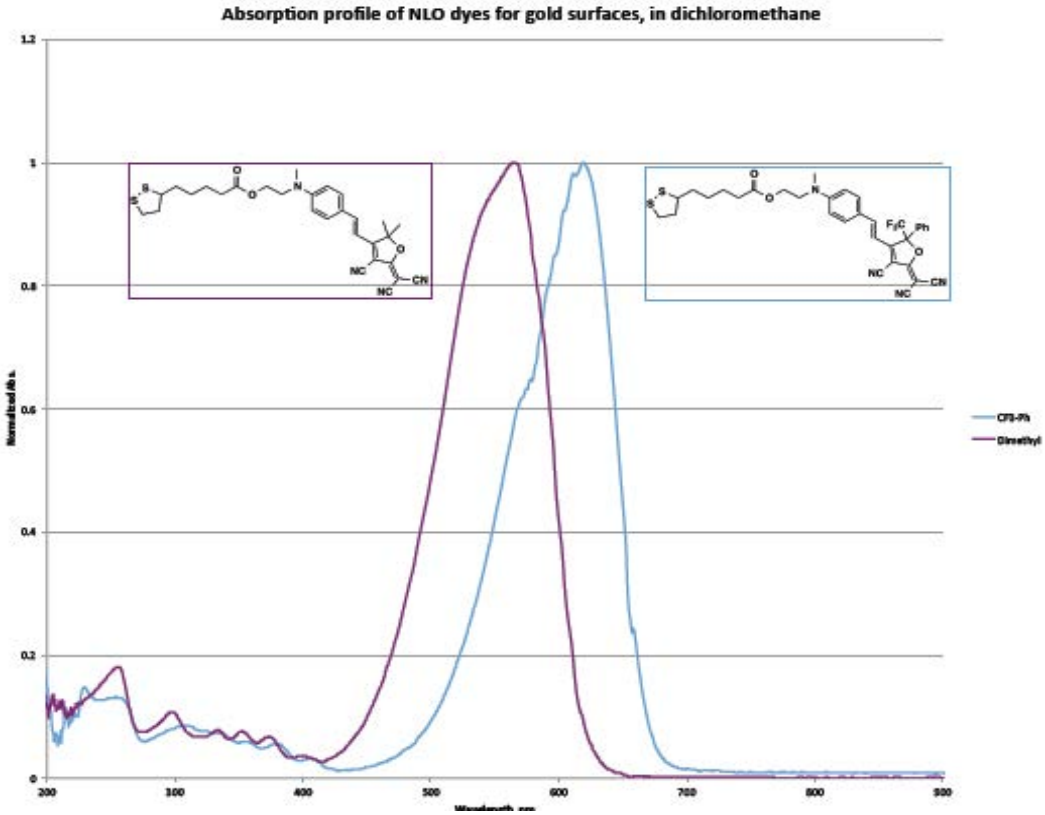

Figure 5.3.1: UV-Visible absorption spectra of ONLO 1 and ONLO 2.

Professor Zayats' group has expertise in preparing highly organized, vertically oriented gold nanorods on various surfaces using a template assisted electrochemical deposition process.(27, 29) The process consists of careful anodization of aluminum films to prepare Al_2O_3 films with highly-ordered nanoscale pores. This structure is then immersed into an electrochemical plating bath. When current is applied, plating occurs only within the pores, whose size and interpore distance is defined by the anodization process. Finally, the Al_2O_3 is removed, leaving free-standing, well organized nanorods on a glass surface. The resulting structures (figure 5.3.2) represent an excellent opportunity to study hybrid organic/metal pre-aligned nanorod structures.

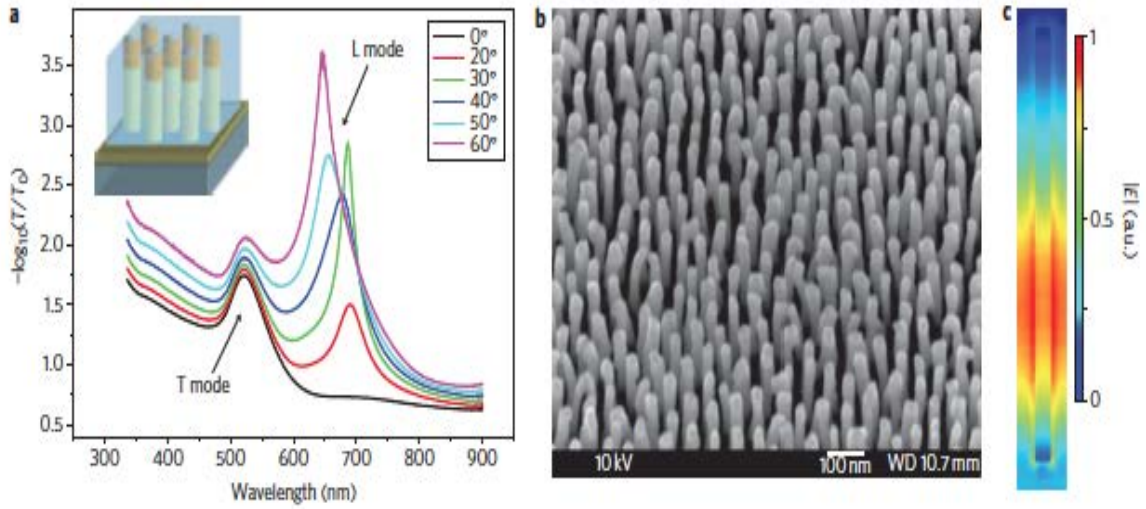

Figure 5.3.2: Plasmonic nanorod metamaterial and its optical properties. **a)** Angle dependant linear extinction of an array of gold nanorods embedded in an alumina matrix. The average length, diameter and center-to-center spacing are 400nm, 20 nm, and 70 nm respectively. **b)** Scanning electron microscopy image of the nanorod assembly **c)** Numerically simulated distribution of the electric field amplitude for strongly interacting gold rods.

Variable angle Polarization Referenced Absorption Spectroscopy (VAPRAS): Using VAPRAS, S-parameters may be determined in order to assess the degree of nanorod orientation obtained by each processing procedure using the relation

$$S = \langle P_2 \rangle = 1/2\left(3\langle \cos^2\theta \rangle - 1\right). \qquad (5.1.3)$$

Here, θ is the angle between the nanorod long-axis and the E-field of light polarized perpendicular to the sample plane (p-polarized). As the sample is rotated to larger angles of incidence, absorption of p-polarized light increases. S and <P_2> may then be determined using

$$\frac{\langle \alpha(\tilde{\nu}) \rangle_p}{\langle \alpha(\tilde{\nu}) \rangle_s} = 1 + \frac{3r\langle P_2 \rangle}{\left(1 - r\langle P_2 \rangle\right) n_{eff}^2(\tilde{\nu})} \cdot \sin^2\theta \qquad (5.1.4)$$

where $\langle \alpha(\tilde{\nu}) \rangle_p$ and $\langle \alpha(\tilde{\nu}) \rangle_s$ are the angle dependent absorption coefficients for the p- and s-optical polarizations respectively. The variable, r, is the anisotropy ratio that relates the orientation of the nanorod transition dipole to the long-axis, and n_{eff} is the effective refractive index. Such a technique may be used to analyze data such as those shown in figure 5.3.2a.

6) Preparation of Improved $\chi^{(2)}$ Materials for Nanocomponent Integration

6.1) – Ferroelectric Liquid Crystal-like materials: Second-order ONLOs currently only achieve about 10-15% of their potential $\chi^{(2)}_{zzz}$ largely due to modest success to-date in induction and and stabilization of long-range unidirectional molecular organization.(28) Molecular organization plays a major role in defining electronic photonic and physical material properties. Therefore, a better understanding of how to create desired long-range order in organic materials, using noncovalent forces, is absolutely essential. The work discussed here addresses this issue through the design of new $\chi^{(2)}_{zzz}$ materials engineered for improved molecular organization. In collaboration with the Bruce H. Robinson Research Lab (University of Washington, Department of Chemistry), we are employing "pseudo-atomistic" rigid body Monte Carlo computational methods to investigate the effects of molecular structure on supramolecular organization, and corresponding $\chi^{(2)}_{zzz}$ values.(30) These computer simulations are being used to provide theoretical guidance for the design of pendant modified ONLO chromophores (PMCs) in order to yield materials with improved (or entirely spontaneous) long-range acentric organization. To date we have selected several target structures and explored the chemical synthesis methods necessary to prepare them. Known highly nonlinear (high β_{zzz}) molecular structures are being modified by the addition of mesogenic pendants in order to mimic the basic structure of organic ferroelectric liquid crystal materials. The structure of such materials is known to intrinsically favor acentric molecular order via an effect commonly referred to as stereo-polar coupling.(31, 32) Stereo-polar coupling takes advantage of both chirality (three- dimensional molecular anisotropy) and unidirectional electrostatic potentials (dipole moments) to create a permanent bulk material polarization. To realize this effect, the dipole axis must be oriented normal to the meosgenic (liquid crystal) axis.(32)

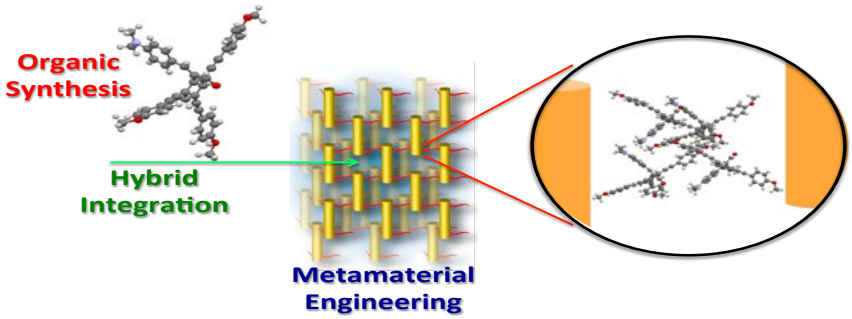

Figure 6.1: Proposed molecular engineering and organic synthesis of rationally designed PMCs, combined with metamaterial engineering to yield NLMMs with unprecedented nonlinear optical properties.

Once prepared and analyzed, we plan on integrating these materials into NLMMs. The goal of this integration will be to realize an overall enhancement of $\chi^{(2)}_{zzz}$ while taking

advantage of the electromagnetic field control offered by the NLMM structure (figure 6.1).

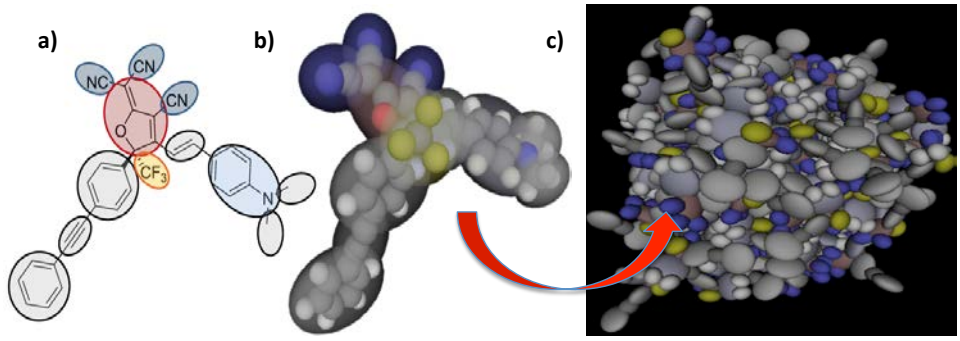

Figure 6.2. (a) Shows the molecular structure of a ferroelectric liquid crystal (FLC) dye overlaid with ellipses indicating "pseudo-atomistic" parameterization. (b) space-filling model of the FLC dye shown for perspective. (c) Depiction of a condensed-phase molecular ensemble of many interacting FLC dyes molecular units.

Interactions among chiral molecules bearing pendant groups is being investigated as a means to further reduce matrix dimensionality (break lattice symmetry). In existing ferroelectric liquid crystals (FLCs), the coupling of asymmetric structure (chirality) and electrostatic interactions (stereo-polar coupling),(31, 33-35) results in the formation of a chiral smectic C* (smC*) phase. In this smC* phase, spontaneous acentric dipolar order arises due to an energetic preference for transverse molecular dipoles to orient unidirectionally along the polar axis of the SmC* phase.(31, 36, 37) In order to create these FLC phases, a neat chiral material may be used, or a chiral dopant may be added to an achiral ordered matrix.(33) This concept of spontaneous symmetry breaking in chiral media has been of interest in the context of EO materials for some time.(32, 36, 38, 39) Indeed, some examples of spontaneous but modest $\chi^{(2)}$, resulting from structural modification of ONLO chromophores, have already been reported(36) (in the context of metamaterials, even a modest spontaneous $\chi^{(2)}$ may be very useful). However, in most modern EO chromophores β_{zzz} and μ_{zz} are oriented collinearly along the long axis of the molecule, while in FLC's the polar axis lies normal to the average molecular long axis (mesogenic axis). This key difference makes it difficult for EO chromophores to realize the correct geometry to take advantage of chiral effects. (32, 36) The chemical structure of a chiral high β_{zzz} PMC is depicted in figure 6.2a. The chemical structure is overlaid with ellipses indicating the approximate pseudo-atomistic parameterization that is being used for Monte Carlo computational modeling. A single tolane pendant is attached at the electron acceptor moiety to create a stereogenic center, inducing asymmetric intermolecular pendant group interactions. The resulting molecular structure, possesses the correct geometry so that acentric order can be favored by stereo-polar coupling (i.e., β_{zzz} and μ_{zz} are oriented transverse to the pendant group).(32, 36) Preliminary Monte Carlo computational simulations Figure 6.2c suggest that in fact a higher degree of e-field induced acentric order is achieved in molecular ensembles of the enantioenriched ONLO relative to the racemic mixture. Additional simulations are currently underway to investigate the possibility of spontaneous ordering and identify promising design modifications.

Scheme 6.1: Synthesis of chiral and achiral Ferroelectric Liquid Crystal-like materials.

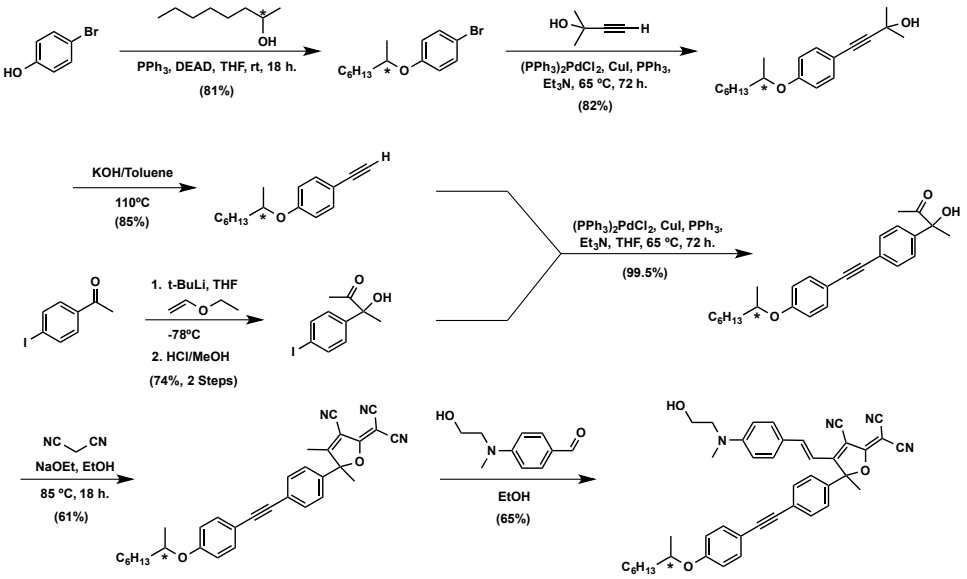

To date, the synthesis of an achiral version of a PMC has been completed via the synthetic approach shown above (scheme 6.1). Thermal data (differential scanning calorimetry) is shown in figure 6.3 (below).

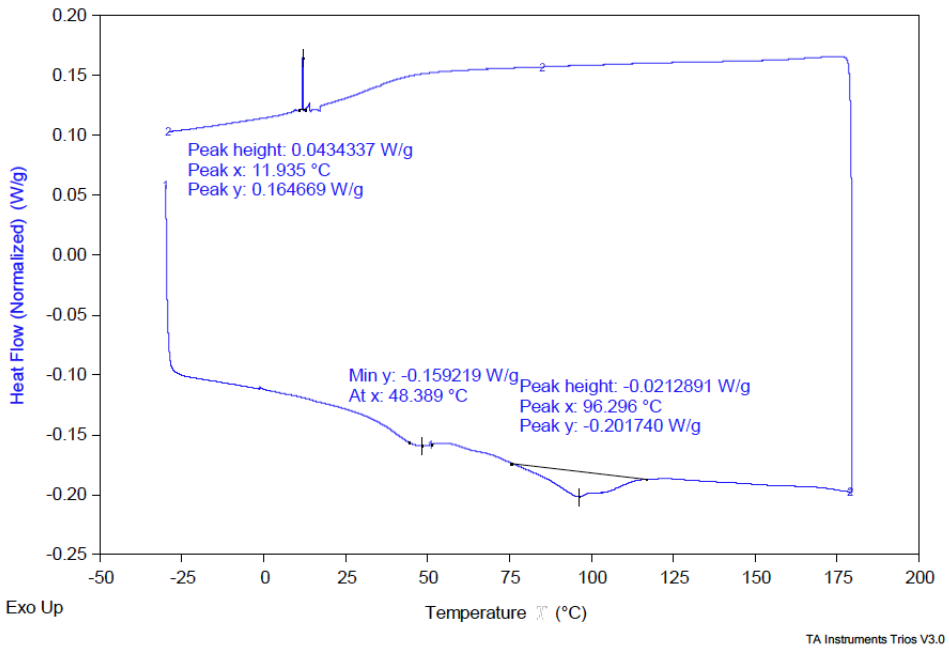

Figure 6.3. Differential scanning calorimetry data showing the thermal transition behavior of PMC 1 (shown above).

6.2) – Ferroelectric Liquid Crystal-like Materials Future Work: New materials made so far and in progress will be analyzed using several techniques in order to assess their physical, chemical and optical (linear and nonlinear) properties. Computer modeling will

be heavily employed in order to analyze results and to guide future structural modifications.

Bibliography:

1. (2009) Metamaterials: transforming theory into reality. *JOSA B* 26(12):B161-B169.
2. (2010) The road ahead for metamaterials. *Science* 328(5978):582.
3. (2013) Lower Poling Thresholds and Enhanced Pockels Coefficients in Nanoparticle-Polymer Composites. *Appl. Phys. Lett.* 103:031102.
4. (2011) A quantitaive study of the enhancement of bulk nonlinearities in metamaterials. *Phys. Rev. A* 84:053805.
5. (2009) Loss as a route to transparency. *Nat. Photon.* 3:75-76.
6. (2014) Hybrid Metal Nanostructure / Organic Nonlinear Dielectric Nonlinear Metamaterials. *In Progress*.
7. (2008) Liquid crystalline phases from polymer functionalised semiconducting nanorods. *J. Mater. Chem.* 18(25):3050.
8. (2010) Orientation and Dynamics of ZnO Nanorod Liquid Crystals in Electric Fields. *Macromol. Rapid Commun.* 31(12):1101-1107.
9. (2009) A robust procedure for the functionalization of gold nanorods and noble metal nanoparticles. *Chem. Commun.*:1724-1726.
10. (1998) Living Free-Radical Polymerization by Reversible Addition-Fragmentation Chain Transfer: The RAFT Process. *Macromolecules* doi:10.1071/CH05072.
11. (2008) Toward Living Radical Polymerization. *Acc. Chem. Res.* 41(9):1133-1142.
12. (2005) Controlling shell thickness in core-shell gold nanoparticles via surface-templated adsorption of block copolymer surfactants. *Macromolecules* 38(14):6115-6121.
13. (2007) Tri-component Diels-Alder polymerized dendrimer glass exhibiting large, thermally stable, electro-optic activity. *J. Mater. Chem.* 17(28):2899-2903.
14. (2007) A Diels-Alder/retro Diels-Alder strategy to synthesize polymers bearing maleimide side chains. *J. Polym. Sci. A Polym. Chem.* 45:4545-4551.
15. (2004) Seed-Mediated Synthesis of Gold Nanorods: Role of the Size and Nature of the Seed. *Chem. Mater.* 16:3633-3640.
16. (2005) Anisotropic Metal Nanoparticles: Synthesis, Assembly, and Optical Applications. *J Phys Chem B* 109(29):13857.
17. (2003) Preparation and Growth Mechanism of Gold Nanorods (NRs) Using Seed-Mediated Growth Method. *Chem. Mater.* 15:1957-1962.
18. (2012) Functional gold nanorods: synthesis, self-assembly, and sensing applications. *Adv. Mater.* 24:4811-4841.
19. (2013) Using binary surfactant mixtures to simultaneously improve the dimensional tunability and monodispersity in the seeded growth of gold nanorods. *Nano Lett.* 13:765-771.

20. (1986) ASE effects in small aspect ratio laser oscillators and amplifiers with nonsaturable absorption. *IEEE Journal of Quantum Electronics* 22:1165-1173.
21. (1999) Amplified spontaneous emission-application to Nd:YAG lasers. *IEEE Journal of Quantum Electronics* 35:101-109.
22. (2006) Y3Al5O12 ceramic absorbers for the suppression of parasitic oscillation in high-power Nd: YAG lasers. *J. Lumiescence* 121:88-94.
23. (2013) Gold nanorods and their plasmonic properties. *Chem. Soc. Rev.* 42:2679-2724.
24. (2012) Nonlinear magnetoelectric metamaterials: Analysis and homogenization via a microscopic coupled-mode theory. *Phys. Rev. A* 86:033816.
25. Boyd RW (2008) *Nonlinear Optics* (Academic Press, Burlington, MA).
26. (2005) Implementing the Theory of Sum Frequency Generation Vibrational Spectroscopy: A Tutorial Review. *Applied Spectroscopy Reviews* 40:103-145.
27. (2011) Designed ultrafast optical nonlinearity in a plasmonic nanorod metamaterial enhanced by nonlocality. *Nature Nanotechnology* 6:107-111.
28. (2010) Electric Field Poled Organic Electro-Optic Materials: State of the Art and Future Prospects Chemical Reviews. *Chem. Rev.* 110:25-55.
29. (2012) Nonlinear Plasmonics. *Nature Photonics* 6:737-748.
30. (2009) Modeling the Optical Behavior of Complex Organic Media: From Molecules to Materials. *J. Phys. Chem. B* 113(47):15581-15588.
31. Goodby JW (1991) Ferroelectric Liquid Crystals: Principles, Properties and Applications. eds Goodby JW, Blinc R, Clark NA, Lagerwall ST, Osipov MA, Pikin SA, Sakurai T, Yoshino K, & Zeks B (Gordon & Breach, Philidelphia), pp 99-157.
32. (1999) Ferroelectric liquid crystals for second order nonlinear optics. *PURE AND APPLIED CHEMISTRY* 71(11):2117-2124.
33. (2005) Ferroelectric liquid crystals induced by dopants with axially chiral 2, 2'-spirobiindan-1, 1'-dione cores. *J. Am. Chem. Soc.* 127(39):13656-13665.
34. (2010) Electro-optic switching and dielectric spectroscopy studies of ferroelectric liquid crystals with low and high spontaneous polarization. *Thin Solid Films* 519(3):1052-1055.
35. (2004) Photoswitching of ferroelectric liquid crystals using unsymmetrical chiral thioindigo dopants: structural effects on polarization photomodulation. *J. Mater. Chem.* 14(9):1486.
36. (2009) Laterally Azo-Bridged H-Shaped Ferroelectric Dimesogens for Second-Order Nonlinear Optics: Ferroelectricity and Second Harmonic Generation. *J. Am. Chem. Soc.* 131(51):18386-18392.
37. (2005) Ferroelectric liquid crystals with fluoro and azafluorenone cores: the effect of stereopolar coupling. *Liquid Crystals* 32(9):1195-1203.
38. (1995) Supramolecular second-order nonlinearity of polymers with orientationally correlated chromophores. *Science* 270(5238):966.
39. (1998) Strong Enhancement of Nonlinear Optical Properties Through Supramolecular Chirality. *Science* 282(5390):913-915.